PHYSICAL REVIEW D

PARTICLES AND FIELDS

Charm photoproduction at 20 GeV

K. Abe,[m] T. C. Bacon,[e] J. Ballam,[k] A. V. Bevan,[e] H. H. Bingham,[o] J. E. Brau,[q] K. Braune,[k]
D. Brick,[b] W. M. Bugg,[q] J. M. Butler,[k] W. Cameron,[e] J. T. Carroll,[k] J. S. Chima,[e]
H. O. Cohn,[i] D. C. Colley,[a] G. T. Condo,[q] S. Dado,[l] R. Diamond,[d]
P. J. Dornan,[e] R. Erickson,[k] R. C. Field,[k] B. Franek,[j] N. Fujiwara,[h]
K. Furuno,[m] R. Gearhart,[k] D. Gershoni,[l] T. Glanzman,[k] I. M. Godfrey,[e]
J. J. Goldberg,[k*] G. P. Gopal,[j] A. T. Goshaw,[c] V. Hagopian,[d] G. Hall,[e]
E. R. Hancock,[j] T. Handler,[q] H. J. Hargis,[q] E. L. Hart,[q] M. J. Harwin,[e]
K. Hasegawa,[m] T. Hayashino,[m] I. Hideta,[m] R. I. Hulsizer,[g] S. Isacson,[l]
M. Jobes,[a] G. E. Kalmus,[j] D. P. Kelsey,[j] J. Kent,[o†] T. Kitagaki,[m]
J. Lannutti,[d] A. Levy,[p] P. W. Lucas,[c] W. A. Mann,[n] R. Merenyi,[n] R. Milburn,[n]
C. Milstene,[p] K. C. Moffeit,[k] J. J. Murray,[k] A. Napier,[n] S. Noguchi,[h]
F. Ochiai,[f] Y. Ohtani,[m] S. O'Neale,[a] A. P. T. Palounek,[c] I. A. Pless,[g]
P. Rankin,[e] W. J. Robertson,[c] A. H. Rogers,[q] E. Ronat,[r] H. Rudnicka,[b‡]
H. Sagawa,[m] T. Sato,[f] J. Schneps,[n] S. J. Sewell,[j] J. Shank,[o] A. M. Shapiro,[b]
R. Sugahara,[f] A. Suzuki,[f] K. Takahashi,[f] K. Tamai,[m] S. Tanaka,[m]
S. Tether,[g] D. A. Waide,[a] W. D. Walker,[c] M. Widgoff,[b] C. G. Wilkins,[a]
S. Wolbers,[o] C. A. Woods,[e] A. Yamaguchi,[m] R. K. Yamamoto,[g] S. Yamashita,[h]
G. Yekutieli,[r] Y. Yoshimura,[f] G. P. Yost,[o] and H. Yuta[m]

[a]*Birmingham University, Birmingham, B15 2TT, England*
[b]*Brown University, Providence, Rhode Island 02912*
[c]*Duke University, Durham, North Carolina 27706*
[d]*Florida State University, Tallahassee, Florida 32306*
[e]*Imperial College, London, SW7 2BZ, England*
[f]*National Laboratory for High Energy Physics (KEK), Oho-machi, Tsukuba-gun, Ibaraki 305, Japan*
[g]*Massachusetts Institute of Technology, Cambridge, Massachusetts 02139*
[h]*Nara Women's University, Kita-uoya, Nishi-Machi, Nara 630, Japan*
[i]*Oak Ridge National Laboratory, Oak Ridge, Tennessee 37830*
[j]*Rutherford Appleton Laboratory, Didcot, Oxon OX11 0QX, England*
[k]*Stanford Linear Accelerator Center, Stanford University, Stanford, California 94305*
[l]*Technion—Israel Institute of Technology, Haifa 32000, Israel*
[m]*Tohoku University, Sendai 980, Japan*
[n]*Tufts University, Medford, Massachusetts 02155*
[o]*University of California, Berkeley, California 94720*
[p]*University of Tel Aviv, Tel Aviv, Israel*
[q]*University of Tennessee, Knoxville, Tennessee 37916*
[r]*Weizmann Institute, Rehovot, Israel*
(SLAC Hybrid Facility Photon Collaboration)

Sixty-two charm events have been observed in an exposure of the SLAC Hybrid Facility to a backward scattered laser beam. Based on 22 neutral and 21 charged decays we have measured the charmed-meson lifetimes to be $\tau_{D^0}=(6.8^{+2.3}_{-1.8})\times10^{-13}$ sec, $\tau_{D^\pm}=(7.4^{+2.3}_{-2.0})\times10^{-13}$ sec and their ratio $\tau_{D^\pm}/\tau_{D^0}=1.1^{+0.6}_{-0.3}$. The inclusive charm cross section at a photon energy of 20 GeV has been measured to be 56^{+24}_{-23} nb. Evidence is presented for a non-$D\bar{D}$ component to charm production, consistent with $(35\pm20)\%$ Λ_c^+ production and some $D^{*\pm}$ production. We have found no unambiguous F decays.

I. INTRODUCTION

In this paper we describe an experiment, performed at the SLAC Hybrid Facility, in which charmed particles were produced and their decays observed.

A 20-GeV backward-scattered photon beam passed through the SLAC 1-m bubble chamber, and downstream detectors were used to trigger the cameras on the total hadronic cross section. The normal three-view stereo cameras were supplemented with a special high-resolution camera to see the decays of the charmed particles clearly separated from their production. Approximately 2.4×10^6 triggered pictures were taken during 80×10^6 expansions of the bubble chamber; these contained about 0.58×10^6 hadronic interactions. After scanning and measuring, 62 events were found containing direct visual evidence for the production and multiprong decay of at least one charmed particle. After imposing rigorous cuts to the data, 51 charm decays remained.

This experiment has several unique features. It investigates the production of charmed particles near threshold using photons. At low energies, where the charged multiplicity is small, the pictures are cleaner than at higher energies; charmed-particle decays can be readily found and their decay topology determined. Two independent methods have shown that the efficiency for finding charmed-particle decays, once cuts have been imposed, is high and uniform. Low incident energy permitted us to use, in the lifetime determination, decays that have missing neutral particles.

Section II describes the equipment and experimental method; Sec. III examines the data, data reduction, and analysis as well as possible backgrounds. In Sec. IV the results on lifetimes of the neutral and charged D mesons, the production cross section, and production mechanisms are discussed. Finally, Sec. V contains our conclusions. Results on lifetimes and the production cross section based on part of the data have been published previously.[1]

II. EXPERIMENTAL DETAILS

A. Beam

The 20-GeV photon beam was produced by back-scattering laser light from 30-GeV electrons provided by the SLAC linear accelerator operated in the SLED (SLAC energy doubler) mode.[2] The burst length was about 100 nsec, and the peak current was typically 50 mA.

A frequency-quadrupled neodymium-doped yttrium-aluminum-garnet laser was used to produce an intense light pulse (~ 50 mJ) with a wavelength of 266 nm and about 10-nsec duration. This light pulse was directed against the electron beam at a crossing angle of 2 mrad. Compton back-scattered photons reached the bubble chamber at a distance of 170 m through a series of collimators and uranium foils (0.3 radiation length). These foils, placed upstream of the collimators and sweeping magnets, eliminated very-low-energy synchrotron radiation. By monitoring the tails of the backscattered beam with a set of four scintillation counters, forming a quadrant detector behind a tungsten collimator, the final steering of the electron beam was continuously and automatically corrected. After collimation, the beam cross section in the bubble chamber was a sharply defined circle of 3mm diam. The outline of the photon beam line is shown in Fig. 1.

Between the quadrant detector and the bubble chamber was a drift-chamber pair spectrometer.[3] A thin copper foil converted about 1% of the incident photons into e^+e^- pairs. This spectrometer was used to obtain a beam energy spectrum (Fig. 2) and provided one measure of the flux.

After passing through the SLAC Hybrid Facility (Fig. 3), the photon beam was absorbed by the beam-stop counter, a lead-lucite sandwich viewed by a phototube. The signal was recorded and used to estimate the flux,
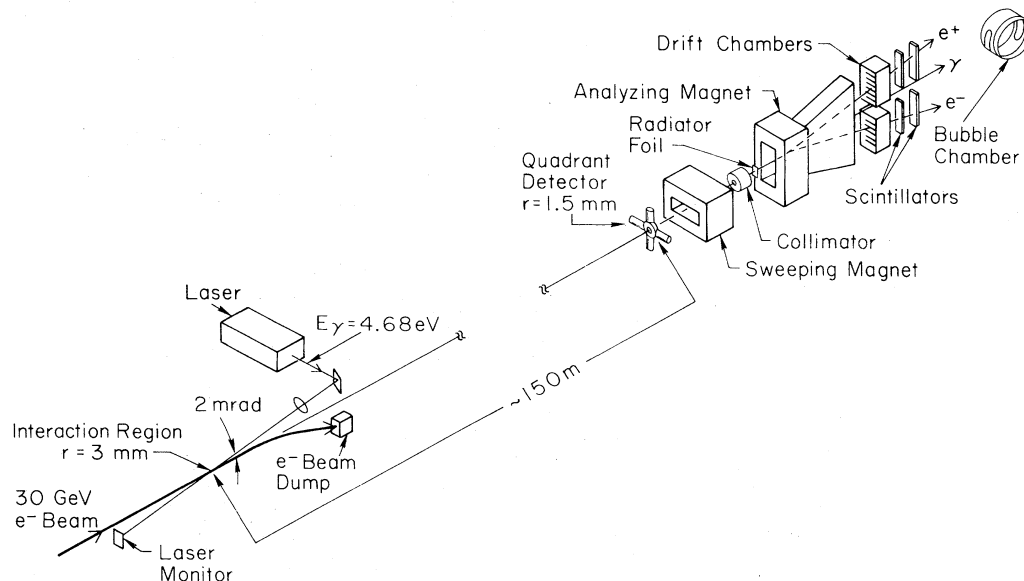

FIG. 1. Layout of the 20-GeV back-scattered laser beam with quadrant detector and pair spectrometer (not drawn to scale).
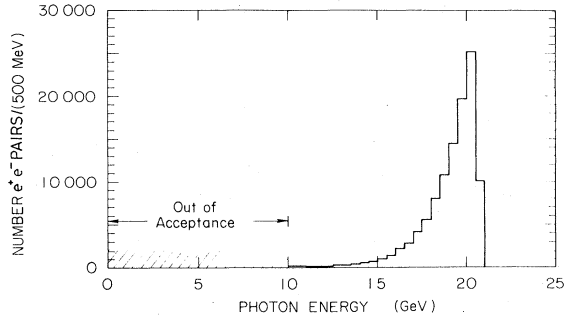
FIG. 2. The photon-energy spectrum (corrected for acceptance) measured by the pair spectrometer.

pulse by pulse. Typically, the beam intensity was in the range 20—30 γ's per pulse.

B. Bubble chamber

The aim of the experiment was to find and measure short decay tracks. In order to achieve small bubble size, two modifications were made to the operation of the SLAC 1-m hydrogen bubble chamber. First, the chamber was operated at about 29 °K, instead of the more normal 26 °K, with as large an expansion ratio as possible. This had the effect of retarding bubble growth and increasing the bubble density. Under these conditions the bubbles grew to ~ 50 μm in about 200 μsec with a bubble density of ~ 60 per cm. Second, the normal stereo triplet was supplemented by a fourth camera which was able to resolve bubbles of this size. This camera was mounted on the central axis of the bubble chamber with a 360-mm focal-length lens (Schneider Componon S) operated at f 11. The camera viewed a length of about 80 cm in the beam plane at a demagnification of 5.5. The corresponding depth of field was about ± 6 mm. The lens was diffraction limited with a resolution of about 45 μm under the above conditions. For this camera, the lights were flashed 200 μsec after the beam entered the chamber. The normal stereo triplet of 125-mm f 22 lenses was also used to photograph the events by triggering separate flash lamps ~ 3 msec after the beam. These cameras were used

to record the events throughout the chamber volume.

Improvements in operation during the experiment included developing the ability to operate the chamber at higher temperatures, the use of a thicker optical window to reduce the thickness of turbulent hydrogen through which pictures were taken, and the introduction of a shutter[4] to prevent light from the later flashes from entering the high-resolution camera.

The chamber ran initially at a repetition rate of 10 Hz and later at 12 Hz.

C. Downstream detectors

The detector system of the SLAC Hybrid Facility consisted of a hydrogen bubble chamber, four sets of proportional wire chambers (PWC's), two threshold Čerenkov counters, and an array of lead-glass blocks. Each of these electronic detectors was made insensitive to background $e^\pm$ pairs in the central (vertical) region.

1. Proportional wire chambers

Each of the first three PWC stations directly downstream of the bubble chamber contained three planes of wires (horizontal, vertical, and diagonal). The fourth PWC was not used in this experiment. The PWC's served two purposes. The first was to provide a trigger for the bubble-chamber camera lamps when a reconstructed track was found to diverge from the e^+e^- pair plane. The second was to improve the momentum measurement of tracks extrapolated from the bubble chamber after film measurement. The momentum resolution for "hybridized" tracks (i.e., both bubble-chamber and PWC measurements used) is

$$\frac{\sigma_p}{p} = [(0.008)^2 + (0.000\,85p)^2]^{1/2} \; ,$$

where p is in GeV/c. Details of the PWC's and the central deadening technique are given in Ref. 5.

2. Čerenkov counters

Two atmospheric-pressure threshold Čerenkov counters[6] were installed behind the PWC's. The first counter was filled with Freon 12 and had a pion threshold of 3.2 GeV/c, and the second one was filled with nitrogen with a pion threshold of 6 GeV/c. The counters each had 12 segments, in two vertical columns, separated by a 10-cm dead region. Using ordinary hadronic events, the acceptance as a function of momentum has been measured and was above 80% for particles with sufficiently high momentum (≥ 3.2 GeV/c) to be well measured by the PWC's (see Fig. 4). Above the effective threshold the efficiency for finding pions was $>97\%$ (see Fig. 5).

3. Lead-glass columns

An electromagnetic calorimeter[7] was located downstream of the Čerenkov counters and is shown in Fig. 6. It was built of 204 lead-glass blocks with a scintillation-counter hodoscope for shower-position measurement after the first 4.3 radiation lengths. There was also a scintilla-
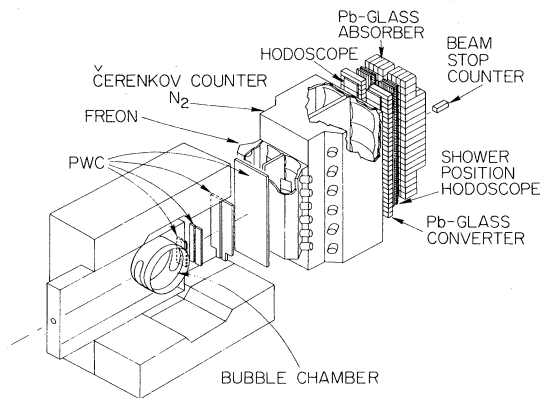

FIG. 3. The SLAC Hybrid Facility with bubble chamber, proportional wire chambers, Čerenkov counters, lead-glass columns, and beam-stop counter.
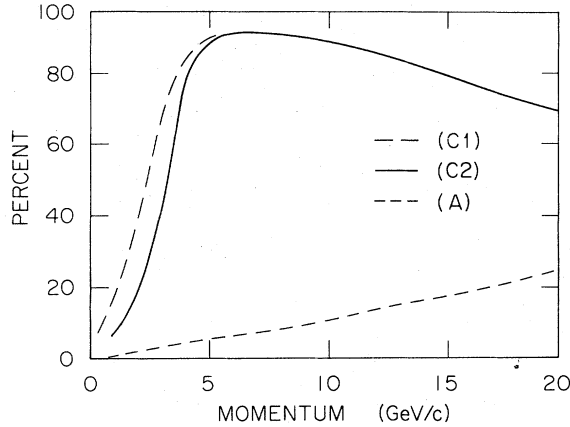
FIG. 4. Acceptance of both Čerenkov counters as a function of particle momentum. With increasing momentum more particles enter the deadened region (see curve labeled A) and therefore the acceptance decreases.

tor hodoscope in front of the calorimeter to detect charged particles. The lead-glass blocks were located behind 1 radiation length of lead, and were separated into an active converter of 3.3 radiation lengths followed by total absorber blocks, which were 10.5 radiation lengths thick at large scattering angles, and 21 radiation lengths thick in the region around the beam. The energy resolution for electrons was measured to be

$$\sigma/E = (0.84 + 4.8/\sqrt{E})\%$$

(E measured in GeV). Figure 7 shows the γ-γ mass spectrum and illustrates the resolution and combinatorial background. Signals from the lead-glass columns were also used to provide a trigger for the bubble-chamber camera lamps.

D. Data acquisition and trigger

As mentioned above, the bubble-chamber cameras were triggered in this experiment. The decision to take a picture was made using information from two basic triggers
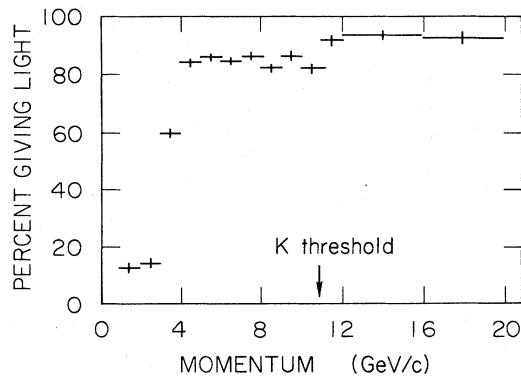

FIG. 5. Fraction of particles giving light in Čerenkov counter 1 as a function of particle momentum.
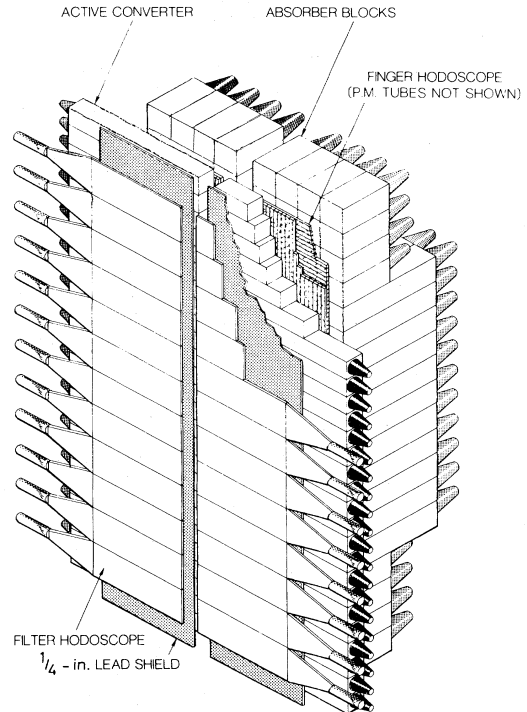

FIG. 6. The lead-glass columns with filter hodoscope (24 counters), lead shield, 52 active converters of lead glass, finger hodoscope (250 counters), and 152 absorber blocks of lead glass.

which were OR-ed together. The first of these used fast analog circuitry to sum the signals from a set of dynodes corresponding to a section of the lead-glass columns. The trigger condition was satisfied if the output signal from such a set corresponded to an energy deposition of more than 2 GeV in the total absorber blocks or 0.8 GeV in the active converter. This trigger was available in less than 2 μsec. The second trigger required a set of hits in the downstream PWC's compatible with a track which originated within the fiducial volume of the bubble chamber. The combinations of three hits which satisfied these criteria were calculated using a software algorithm running in a 168/E emulator.[8] Approximately 100 μsec was needed for this decision.
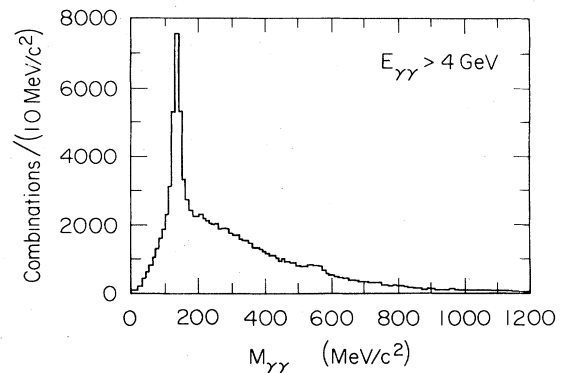

FIG. 7. Inclusive γ-γ mass spectrum for the lead-glass columns.
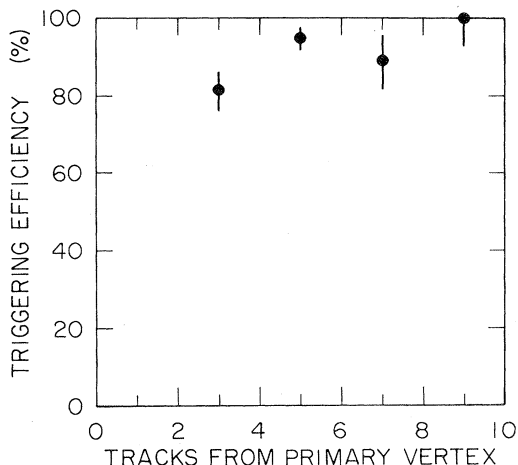
FIG. 8. Variation of triggering efficiency with charge multiplicity.

In addition to the triggered pictures, every 50th frame was taken untriggered. This enabled the triggering efficiency as a function of topology to be measured in an unbiased way. Figure 8 shows the variation of triggering efficiency as a function of the number of tracks coming from the primary vertex. The lead-glass trigger was more efficient at triggering on low-charged-multiplicity events, while the PWC trigger was more efficient for high charged multiplicities. The effect of combining the two was to minimize variations in the trigger efficiency as a function of topology.

The fraction of the beam pulses accepted by the triggers varied during the experiment from 1 in 15 pulses to 1 in 40 pulses depending on the photon flux and the size of the deadened regions in the downstream detectors. The fraction of the pictures taken which contained a hadronic interaction varied from 1 in 10 to 1 in 3.5, depending mainly on the size of the deadened region.

III. DATA

A. Scanning and measuring

The results presented here are based on five experimental runs (see Table I). A total of 2.4×10^6 photos was taken containing approximately 580 000 hadronic interactions. A fiducial volume was defined to eliminate regions

of poor visibility due to flash lamp flares and also to yield good momentum measurement. For the first four runs the length of the fiducial volume along the beam direction was 57 cm. For run 5, the fiducial volume length was increased to 69 cm as some of the flash lamp flares had been removed by the installation of a rotating shutter[4] in the high-resolution camera.

The film from the high-resolution camera was scanned twice, and all hadronic events in the restricted fiducial volume (a total of 378 000) were recorded. Each of these hadronic events was closely examined in two separate passes, at a magnification of about 10× space, for the decays of short-lived particles close to the interaction vertex. Approximately 50% of the film was scanned out to a distance of 3 cm in space while the other 50% was scanned out to 1 cm. All charm candidates (see next section) were measured on the three low-resolution views as well as on the high-resolution view. Events were then passed through a processing chain consisting of geometry (TVGP or HYDRA), hybrid, and kinematics (SQUAW, GRIND, or RUTHERFORD KINEMATICS).

B. Selection and treatment of candidates

In order for an event to be considered a charm candidate, either the decay point had to be clearly visible or the backward projection of one of the tracks in the event had to miss the production vertex by an impact distance of at least one track width (55 μm) (see Fig. 9). All charm candidates found in this way by scanners were then examined by physicists before further processing.

The remaining candidates were measured. Events containing only decays consistent with strange particles or photon conversions were rejected, leaving a sample of events which were thought to be charm. These events were then carefully reexamined by physicists.

High-magnification (at least 20× space) photographic prints were made of each event and measurements of the projected decay length and impact distances were made. Particles were identified, whenever possible, using the two Čerenkov counters and ionization density on the high-resolution photographs.

The following cuts were applied to the events to ensure that the decays which survived were genuine charm decays.

(i) Decays with fewer than two charged products were rejected.

TABLE I. Details of experimental runs.

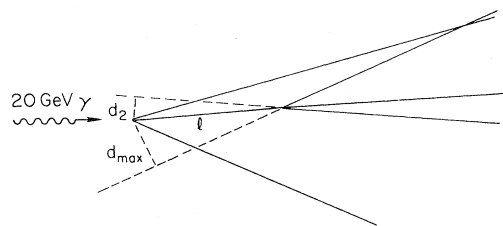| Run no.	Number of pictures taken (10^3)	Total hadronic events (10^3)	Events in fiducial volume (10^3)	Length of fiducial volume (cm)
1	92	11	7	57
2	445	84	52	57
3	636	161	100	57
4	806	180	112	57
5	429	144	108	69
Total	2408	580	378	

FIG. 9. Sketch showing the decay parameters used in the analysis; maximum projected impact distance (d_{max}), second largest projected impact distance (d_2), and projected decay length (l).

TABLE II. Details of the 72 charmed-particle decays. The charged multiplicity is the number of charged tracks from the decay of the charmed particle. For charged decays the sign shown is the charge of the charmed particle. The decay parameters (d_{max}, d_2, l, p', l_{eff}, and T_{eff}) are defined in Secs. III B and IV A. Decays which fail the cuts have no entry in the l_{eff} or T_{eff} columns.

(a) Charged decays

Event	Charged multiplicity	d_{max} (μm)	d_2 (μm)	l (mm)	p' (GeV/c)	l_{eff} (mm)	T_{eff} (10^{-13}sec)
596-237	+3	480	285	1.95	9.7	1.45	9.3
781-275	−3	374	372	1.42	9.9	0.92	5.8
916- 16	−3	139	52	1.61	11.3	0.34	1.9
958-596	−3	190	135	1.34	9.8	0.56	3.6
1002-194	−3	200	70	1.30	8.8	0.56	3.9
1187-229	+3	244	168	1.02	8.4	0.52	3.8
1293-147	+3	1033	303	3.41	6.1	2.91	29.6
1303-179	−3	190	160	1.34	11.8	0.56	3.0
1415-225	+3	1531	263	1.73	10.0	1.23	7.7
1562-192	−3	200	65	0.65	10.0	0.15	0.9
1574-761	−3	540	540	3.70	8.0	2.95	23.1
1795-159	−3	112	91	1.53	16.5	0.03	0.1
1893-388	−3	580	320	1.07	8.0	0.57	4.5
1914-741	−3	1243	310	4.08	9.8	3.55	22.7
1960-760	−3	146	91	0.96	11.6	0.24	1.3
2256-764	+3	694	266	1.92	5.4	1.42	16.5
2332-897	−3	1225	235	1.66	7.9	1.16	9.1
2407-337	+3	387	142	0.61	10.0	0.11	0.7
2501-432	−3	220	110	0.65	4.6	0.15	2.0
2703-110	+3	340	65	0.59	4.1	0.09	1.4
2979-652	−5	825	90	1.73	11.7	0.96	5.1
3000-582	−3	360	210	0.48	2.6		

(b) Neutral decays

Event	Charged multiplicity	d_{max} (μm)	d_2 (μm)	l (mm)	p' (GeV/c)	l_{eff} (mm)	T_{eff} (10^{-13} sec)
435-714	2	70	0	0.54	8.2		
435-714	2	246	246	1.45	4.9	0.80	10.2
437- 27	2	80	53	0.69	4.9		
437- 27	2	534	267	2.51	11.2	1.99	11.1
636-188	2	403	50	0.90	11.1	0.18	1.0
944- 15	2	213	14	1.05	6.6		
944- 15	4	240	180	1.60	8.1	0.87	6.6
994-845	4	320	160	1.45	11.1	0.95	5.3
1079-160	2	170	133	1.07	8.4	0.38	2.8
1187-229	2	890	45	1.94	5.1	0.22	2.6
1240-429	2	80	0	0.70	10.6		
1256- 3	2	795	235	2.24	6.7	1.74	16.1
1285-919	4	625	255	4.92	12.4	4.05	20.4
1404-883	4	680	390	1.68	7.2	1.18	10.2
1466-325	2	324	226	2.39	6.0	1.58	16.2

(ii) Decays consistent either with photon conversions or strange particles were rejected. In order to reduce the background from strange-particle decays to a negligible level the following cuts were applied (see Sec. III D). The two-body (assumed to be $\pi\pi$) invariant mass had to be greater than 550 MeV/c^2 and be more than 5 standard deviations above the K^0 mass in order to be accepted. This cut removed K^0 decays. Analogous criteria were used to remove Λ, $\overline{\Lambda}$ decays ($m_{p\pi} > 1130$ MeV/c^2 and more than 5 standard deviations above the Λ mass) and $\gamma \rightarrow e^+e^-$ conversions ($M_{e^+e^-} > 50$ MeV/c^2).

(iii) Three-prong decays consistent either with $K^\pm \rightarrow \pi^\pm \pi^+ \pi^-$ or $\Sigma^+ \rightarrow p\pi^0$ ($\pi^0 \rightarrow e^+e^-\gamma$) were rejected, as were decays consistent with a neutral-strange-particle decay superimposed on a track from the production vertex.

A total of 62 events remained, which contain 72 visible multiprong charm decays. Fifty seven of the 72 decays are topologically unambiguous. The remaining 15 decays are ambiguous between charged and neutral decays. Table II contains details of the 72 decays. Figure 10 shows two of the events found.

TABLE II. *(Continued.)*

Event	Charged multiplicity	d_{max} (μm)	d_2 (μm)	l (mm)	p' (Gev/c)	l_{eff} (mm)	T_{eff} (10^{-13} sec)

(b) Neutral decays (continued)

Event	Charged multiplicity	d_{max} (μm)	d_2 (μm)	l (mm)	p' (Gev/c)	l_{eff} (mm)	T_{eff} (10^{-13} sec)
1502-157	4	60	51	0.43	14.3		
1669-911	2	93	0	0.85	11.9		
1741-352	2	507	80	3.03	10.1	1.52	9.3
1997-398	4	186	112	1.07	8.7	0.44	3.1
2053-318	4	896	59	1.30	6.0	0.42	4.4
2301- 98	4	48	21	0.24	8.7		
2328-961	2	180	55	0.91	11.7	0.25	1.3
2529-268	4	150	110	1.33	12.9	0.35	1.7
2567- 64	2	320	100	0.70	5.8	0.20	2.2
2622-970	4	280	260	1.39	9.3	0.84	5.6
2652-714	4	165	150	1.00	11.3	0.33	1.8
2693-360	4	400	50	1.96	7.9	0.39	3.1
2727-638	2	192	13	0.52	9.5		
2817-847	2	53	50	0.26	8.1		
2817-847	2	40	0	0.31	10.2		
2913-429	2	111	37	0.96	10.5		
2913-429	2	176	19	0.65	6.5		
2977-354	4	317	185	0.98	9.1	0.48	3.3
2998-880	4	41	32	0.49	11.9		
2998-880	2	350	158	0.91	5.8	0.41	4.4

(c) Charged/neutral ambiguous decays

Event	Charged multiplicity	d_{max} (μm)	d_2 (μm)	l (mm)	l_{eff} (mm)
352-631	2/+3	971	226	2.16	1.66
773- 40	2/−3	215	80	0.59	0.09
781-275	2/+3	237	118	0.56	0.06
1216- 85	2/−3/+3	62	40	0.30	
1216- 85	4/4	80	80	0.72	
1344-119	−3/4/−5	165	140	0.41	
1573-278	+3/4/−5/+5	303	168	0.90	0.40
1783-636	4/−5/+5	215	160	0.45	
2240- 10	2/−3/+3/4	726	160	2.77	2.08
2240- 10	+3/4/+5	160	144	0.37	
2526-327	2/−3/+3/4	121	40	0.24	
2599-516	−3/4	138	65	0.57	0.07
2712-354	4/−5	480	110	1.95	1.24
2850-290	2/−3/+3/4	370	50	1.32	0.26
2998-163	2/+3/4	190	40	0.38	

Further cuts were applied to ensure that events were detected with uniform and high efficiency and to reduce the number of ambiguous decays. The values of these cuts were chosen to ensure that reasonable variation in their values did not change any conclusions reached on lifetimes or cross section. The cuts chosen were as follows (see Fig. 9):

(iv) A minimum-projected-decay-length cut of 500 μm was imposed.

(v) A projected impact distance d_{max} greater than 110 μm (two track widths) was required for at least one track in a decay.

(vi) Another projected impact distance d_2 greater than 40 μm was required for a second track from the same decay vertex.

After these cuts were applied 49 events remained con-

taining 51 decays [one additional decay consistent with being a one-prong, i.e., failing cuts (i) and (vi), is contained in the 49 events]. Forty three of the 51 decays are topologically unambiguous (22 neutral, 21 charged) and eight are charged/neutral ambiguous (see Table II).

C. Scanning and triggering efficiencies

All of the film was scanned twice for hadronic interactions. For each event, information was recorded as to whether it was found on the first scan and/or second scan. Based on this information the combined scanning efficiency for finding multiprong hadronic interactions was found to be (99±1)%.

These hadronic interactions were then scanned twice on the high-resolution film to find charm candidates. Again,
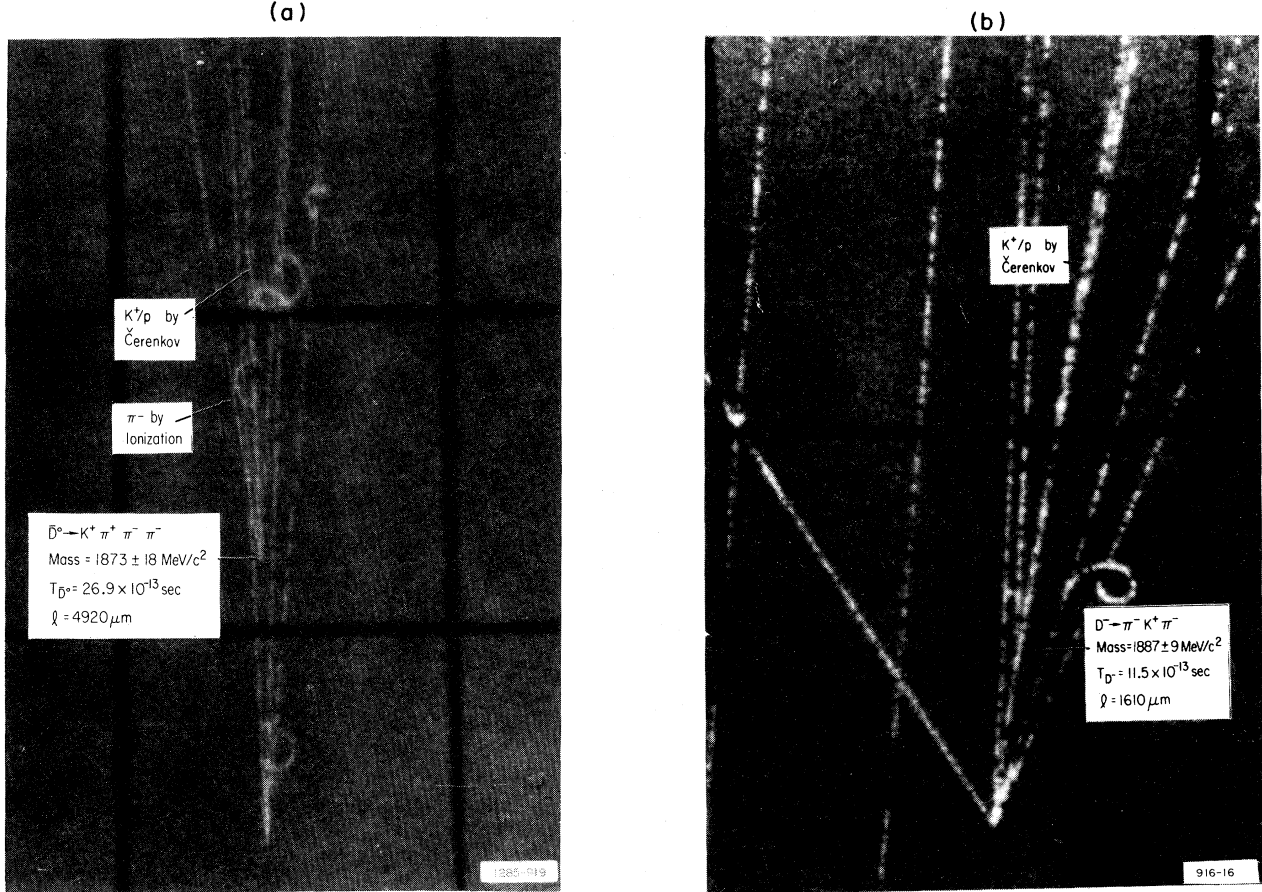
(a) (b)

FIG. 10. Photographs of two events taken by the high-resolution camera. Note that the time shown is the actual flight time, not an effective lifetime. (a) Neutral fully reconstructed $\bar{D}^0 \rightarrow K^+\pi^+\pi^-\pi^-$. (b) Charged fully reconstructed $D^- \rightarrow \pi^- K^+ \pi^-$.

information was recorded on which candidates were found on each scan. Based on the 49 charm events which pass all of the cuts, the efficiency for finding charm events was calculated to be $(92\pm4)\%$ using the method of Derenzo and Hildebrand.[9]

As a further check on the efficiency for detecting decays close to the primary vertex, the decay length and impact-distance distributions were studied for short-lived K^0's and Λ's, which have great visual similarity to neutral D decays into two charged particles. The data sample used was collected during the scanning for charm on the high-resolution film and consisted of V^0's having projected decay lengths of up to 5 mm and with at least one impact distance less than 700 μm.

A Monte Carlo method was used to predict the shapes of each of these distributions. In order that no model dependence be introduced by this, the kinematic information for a large sample of K_S^0 and Λ decays found throughout the fiducial volume of the chamber was used as input. These were then given the conventional acceptance weight to take into account losses at short decay lengths and outside the fiducial volume in order to make the sample unbiased. Each such V^0 was assigned a random projected decay distance l between 0 and 5 mm from the primary vertex along its true line of flight. Assuming this new decay position relative to the production vertex,

the corresponding impact distances for the tracks from the V^0 were calculated from their known direction vectors. To obtain the correct lifetime dependence a further weight was applied to each V^0 corresponding to the probability that it would decay at its assigned distance l' from the vertex. This probability is given by

$$P(l') = (m/pc\tau)\exp(-l'm/pc\tau) ,$$

where m, p, and τ are the mass, momentum, and mean proper lifetime of the particle, respectively, and c is the speed of light. The weight used was the reciprocal of $P(l')$. In this way, the four-vector for each real V^0 could be used as many times as necessary in order to obtain smooth distributions.

Figure 11(a) shows the comparison of the projected decay length (l) of the V^0's with the Monte Carlo prediction. In both the data and the Monte Carlo samples, V^0's with d_{max} less than 110 μm were eliminated in order that the efficiency at small lengths could be examined independently of that for d_{max}. The Monte Carlo is normalized to the data outside the first two bins (which corresponds to the region affected by the l cut). In these two bins, it can clearly be seen that the data come very close to the predicted levels indicating a high efficiency below the cut.

Figure 11(b) shows the corresponding plots of d_{max} for the V^0 sample, this time with the cut ($l > 0.5$ mm) ap-
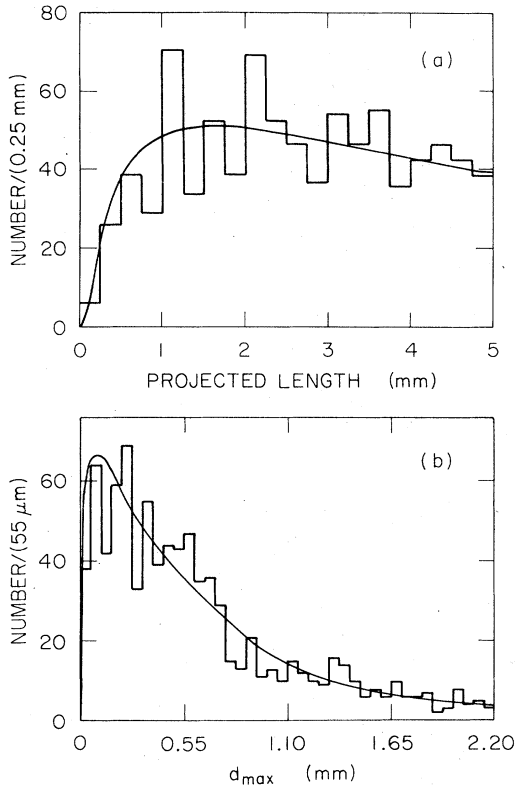
FIG. 11. Comparison of short K_S^0 and Λ decay distributions with a Monte Carlo prediction. (a) shows the length (l) distribution for V^0's with $d_{max} > 110$ μm and (b) is the d_{max} distribution for V^0's with $l > 0.5$ mm. In each case the prediction is shown superimposed as a solid curve normalized to the data outside the first two (cut-affected) bins.

plied to the data. The binning again is such that the first two bins cover the range $0 < d_{max} < 110$ μm. These plots confirm that the scanning efficiency of short V^0's passing the cuts is high and uniform.

The triggering efficiency for hadronic events was determined by taking every 50th frame of film untriggered during the course of the experiment. By processing the events found in the untriggered film through the trigger algorithm, the triggering efficiency for hadronic events was determined as a function of charge multiplicity (see Fig. 8). The charm triggering efficiency was then deduced from this by using the multiplicity distribution of the charm events and assuming that their efficiency is the same as for normal hadronic events of the same multiplicity. For the first four runs the charm triggering efficiency was determined to be $(92\pm4)\%$. During run 5, the downstream detectors had a wider central dead region, so the charm triggering efficiency for this run was lower and was determined to be $(76\pm8)\%$. The weighted-average charm triggering efficiency for the whole experiment was $(87\pm4)\%$.

D. Backgrounds

Two approaches have been used in estimating the background to our charm signal. First, direct measurements have been made and second, calculations based on many possible sources have been carried out. Both methods give limits of less than one background neutral or charged decay in the entire experiment.

In the direct measurement, a reference region in space that contained no charmed particles but all possible sources of background, was chosen very close to the region populated by the charmed-particle decays, and we call this the background region. All the hadronic events on the high-resolution view were scanned out to 10 mm in space from the vertex and 50% of the film out to 30 mm. Since all charm candidates which passed the cuts occurred within the first 5 mm, the region 5–10 mm (or 5–30 mm in 50% of the film) can be regarded as a charm-free region. By noting how many events passed the cuts in this region and estimating how any background process might vary between the charm region (0.5–5 mm) and the background region (5–10 or 5–30 mm), an upper limit for background to both neutral and charged decays was found.

In our experiment we observed neutral decays into two and four prongs and charged decays into three and five prongs.

1. Two-prong decays

(i) The majority of two-prong "decays" that are seen in this experiment come from the decays of K_S^0 and Λ's and from γ conversions to $e^\pm$ pairs; also some can come from K_L^0 decays. These backgrounds were eliminated by means of the mass cuts discussed in Sec. III B.

These cuts also eliminated some real D^0's and in Sec. IV B their effect is taken into account.

There are two other possible sources of background to two-prong decays which might not be eliminated by these mass cuts.

(ii) A secondary interaction of a neutral particle (K^0, Λ, or n), emitted from the primary vertex, in which one of the prongs (proton) is not seen, e.g., $np \rightarrow (p)p\pi^-$. This source of background is estimated to be much less than one event.

(iii) Two primary beam photon interactions very close to each other where the downstream interaction is an apparent two-prong interaction (e.g., low-P_T ρ production). This background source is eliminated by the condition that the total visible longitudinal momentum of the event be less than the maximum beam momentum.

2. Four-prong decays

Most strange-particle decays do not form a possible topological background although rare processes such as $K_L^0 \rightarrow \pi^+\pi^-\pi^0$ ($\pi^0 \rightarrow e^+e^-\gamma$) could contribute in principle. Processes of types (ii) and (iii) above could also contribute.

However, no two-prong or four-prong event which passed all the cuts imposed on charmed-particle candidates (including the mass cuts) survived beyond 5 mm from the primary vertex.

The significance of this result was calculated as follows.

If the total path searched in the signal region $(5-0.5)$ mm $= N_h(4.5)$ mm, and the total path searched in the background region $= N_h(10.0-5.0)$ mm $+ 0.5N_h(30.0-10.0)$ mm (where N_h is the number of

hadronic interactions in the experiment), and if the background were distributed uniformly along the 10-mm (or 30-mm) path length searched, then

$$\frac{\text{background path length}}{\text{signal path length}} = \frac{15N_h}{4.5N_h} = 3.3 \ .$$

We have investigated the possibility that the background might not be uniformly distributed. For the K^0 and Λ decays we find a small decrease with distance (there are $\sim 25\%$ fewer K^0 and Λ decays between 15 and 30 mm than between 0 and 15 mm) and therefore the ratio of 3.3 is reduced to 2.7. For the other sources [(ii) and (iii)] there is no evidence for any significant departure from uniformity. Therefore, there is less than one background event in our D^0 sample (90% C.L.).

3. Three-prong decays

Three types of background sources can be envisioned, all of which are expected to be small.

(i) Decays of charged strange particles into three-body final states,

$$K^\pm \rightarrow \pi^\pm \pi^+ \pi^- \ , \tag{1}$$

$$K^\pm \rightarrow \pi^\pm \pi^0 (\pi^0 \rightarrow e^+ e^- \gamma) \ , \tag{2}$$

$$K^\pm \rightarrow e^\pm \nu_e \pi^0 (\pi^0 \rightarrow e^+ e^- \gamma) \ , \tag{3}$$

$$K^\pm \rightarrow \mu^\pm \nu_\mu \pi^0 (\pi^0 \rightarrow e^+ e^- \gamma) \ , \tag{4}$$

$$\Sigma^\pm \rightarrow p \pi^0 (\pi^0 \rightarrow e^+ e^- \gamma) \ . \tag{5}$$

All three-prong charmed-particle candidates were subjected to two cuts. First, that $M_{\pi\pi\pi}$ be more than 3σ above M_K. Second, that no two tracks in the decay be consistent with electrons whose invariant mass $M_{e^+ e^-}$ was less than 100 MeV/c^2. These cuts reduced the background from the decays (1)–(5) to a very small level.

(ii) A secondary interaction of a charged particle from the primary vertex which resulted in a four-prong event in which a short positive prong was not seen.

(iii) K^0 or Λ decays whose vertices lie on top of outgoing charged tracks and therefore look like three-prong decays. In order to eliminate this background, the invariant mass of the pairs of positive and negative particles was calculated. The candidate was rejected if $M_{\pi^+ \pi^-}$ was less than 550 MeV/c^2, or $M_{p\pi}$ was less than 1130 MeV/c^2, or within 5σ of M_{K^0} or M_Λ, and if the remaining track (the one not involved in the invariant mass) went straight back to the production vertex.

4. Five-prong decays

In this case only the background due to secondary interactions is possible, i.e., a secondary six-prong interaction in which one positive prong is not seen.

After all the cuts had been imposed, no candidate three-prong or five-prong decay remained at distance greater than 5 mm from the production vertex. As in the case of the neutral background, the ratio

$$\frac{\text{background path length}}{\text{signal path length}} = 3.3 \ .$$

In this case the only background which may not be constant over the first 10 (or 30) mm is type (iii), where the chance of a K^0 or Λ lying on top of an outgoing charged track is greater close to the production vertex than far away. In fact, the probability for this happening should be inversely proportional to distance, so that any K^0's or Λ's which survive the mass cuts are more likely to lie on an outgoing track close to the vertex than further away.

Thus, for type-(iii) background, the ratio

$$\frac{\text{effective background path length}}{\text{signal path length}} \sim 0.6$$

and not 3.3, as above. This limit can be reduced by noting that this background can only occur if a high-mass (above 550 MeV/c^2) V^0 lies on top of an outgoing track from the primary vertex. Since we have already noted that the number of high-mass V^0's in the background region is zero, leading to an upper limit of less than 1 background high-mass V^0 in the signal region, the limit for high-mass V^0's overlaying outgoing tracks must be even lower than this. Therefore the background to the charged charm-particle signal is less than one event at the 90% C.L.

As a final check, detailed calculations, with the same cuts imposed, were made of a large number of potential background sources to both the charged and neutral decays. These confirmed the direct observation that the background is less than one event for our sample of charged or neutral decays.

IV. RESULTS

A. Lifetimes

After the cuts described in Sec. III B were imposed, 49 events remained containing 51 decays satisfying all six conditions. This sample includes 22 neutral (11 two-prong and 11 four-prong decays), 7 positive (all three-prong decays, but one with an additional Dalitz pair), 14 negative (13 three-prong decays and one five-prong decay), and 8 charged/neutral ambiguous decays. Eight of the neutral and 11 of the charged decays are compatible with Cabibbo-allowed D decays with no missing neutral particles; the rest are compatible if a missing π^0, K^0, or ν, or a Cabibbo-unfavored decay is assumed. In most cases, not all charged tracks are identified. Thus, when considering individual $D^\pm$ candidates, the $F^\pm$ hypothesis cannot be excluded, and for 5 of the 7 positive decays, Λ_c^+ is also possible. There is, however, good evidence that most of the charged decays we see are in fact D mesons (see Sec. IV C).

Despite the lack of complete neutral-particle detection, the relatively low beam energy allowed us to obtain narrow limits on the momentum used for the lifetime determination.

The lifetime is determined by comparing a set of parameters describing each decay to those of Monte Carlo events. The same cuts (see Sec. III B) were applied to the Monte Carlo events as to the data. The parameters used to describe the decays were as follows.

(i) d_{max}, the maximum impact distance among the decay tracks.

(ii) l, the actual projected distance traveled by the charmed particle as measured on the high-resolution picture.

(iii) l_{eff}, the actual distance (l) traveled by the particle, minus the length from the production vertex to the first point along its path where its decay would have satisfied the acceptance conditions (iv), (v), and (vi) of Sec. III B. These lengths were projected onto the film plane. Note that this first detection point is uncorrelated with the decay distance itself. Thus, l_{eff} is the path length over which a charmed particle would have been accepted as such.

(iv) T_{eff}, the average effective lifetime calculated by using upper (P_{max}) and lower (P_{min}) limits on the momentum for each decay to estimate the real momentum. The lower limit of the momentum is the momentum sum of the visible particles in the decay and the upper limit is obtained by assuming all of the neutral momentum in the event comes from the charm decay vertex. Then,

$$\frac{1}{P'} = \frac{1}{2}\left[\frac{1}{P_{max}} + \frac{1}{P_{min}}\right]$$

and

$$T_{eff} = \frac{l_{eff}M}{P'c},$$

where M was taken to be the D mass. Because of the relatively low beam energy the P_{min} and P_{max} are normally close in value. The fully reconstructed nature of some decays has been ignored in computing P_{min} and P_{max}.

Figure 12 gives the experimental distributions of d_{max}, d_2, and l; Fig. 13 gives the distributions of l_{eff} and T_{eff}. In comparing the charged and neutral decays, note the similarities in the distributions. The distributions of the total visible momentum in the decay were also similar (see Sec. IV C). The distributions of the ambiguous decays are compatible with both the charged and neutral distributions, and if added to either sample change the lifetime by less than $\frac{1}{4}$ of the error.

The maximum-likelihood determination of the lifetimes (where the parameters l, l_{eff}, d_{max}, and T_{eff} are compared to Monte Carlo events on an event-by-event basis) yields the likelihood curves shown in Fig. 14. After the sys-
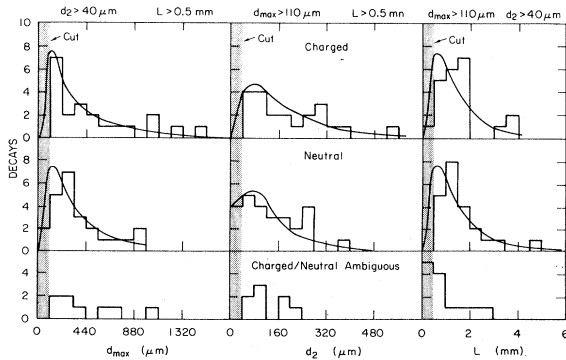

FIG. 12. Distributions of d_{max}, d_2, and l. The curves are from Monte Carlo calculations using the charged and neutral lifetimes given in the text, normalized to the number of events.
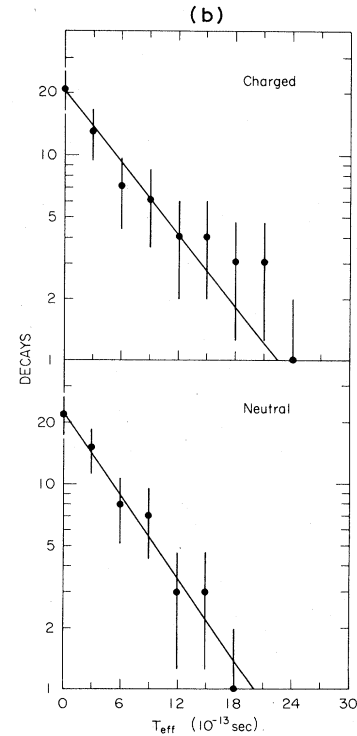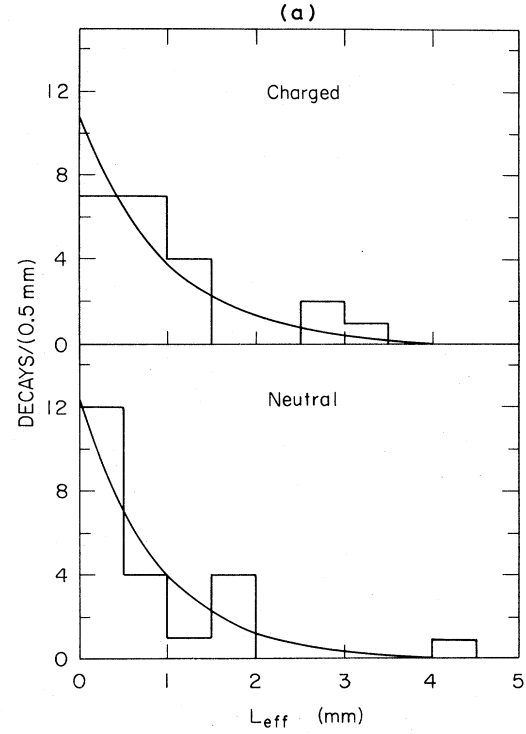

FIG. 13. (a) Distribution of l_{eff} and (b) cumulative distribution of T_{eff} for the charged and neutral decays. The curves are exponentials representing the charged and neutral lifetimes given in the text, normalized to the number of decays.
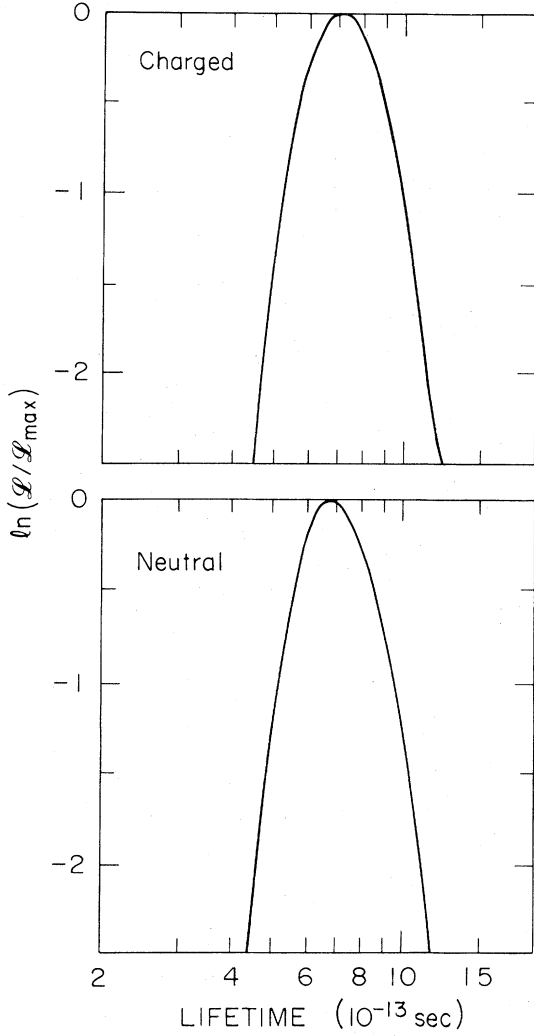
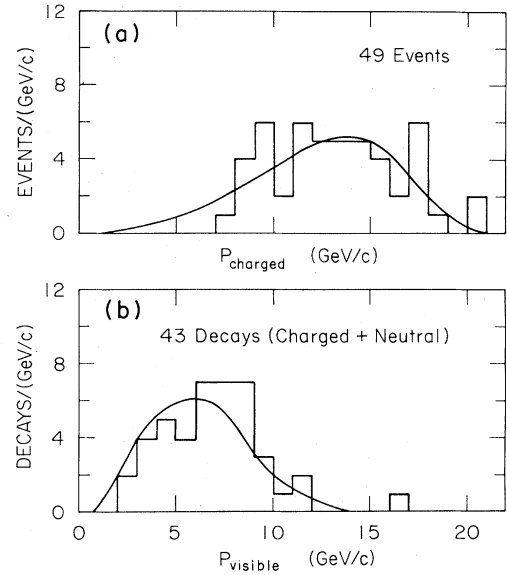FIG. 14. Logarithmic-likelihood curves for the charged and neutral decays.

FIG. 15. (a) Total charged momentum in the event for the 49 events in which at least one decay passed all the cuts. (b) Total visible momentum in the decay for the 43 topologically unambiguous decays. The curves are the predictions from the model used in the Monte Carlo.

rameters d_{max}, T_{eff}, l, and l_{eff}, as well as the lifetime determined from the fully reconstructed decays. It can be seen from the table that each value is consistent with the maximum-likelihood calculation.

The sensitivity of these lifetime values to the particular choice of cut parameters has been determined by increasing the cut parameters and recomputing the lifetimes. This procedure was performed in a number of ways, always indicating that the cuts of Sec. III B had removed the bias against short decay lengths. Figure 16 shows the results of one such test where the cuts were all changed by the same factor F (e.g., $F=2$ refers to $d_{max} > 220$ μm, $d_2 > 80$ μm, and $l > 1.0$ mm). As the factor is increased the computed value of lifetime using the maximum-

tematic errors are combined with the statistical errors, which are dominant, we find

$$\tau^{\pm} = (7.2^{+2.3}_{-2.0}) \times 10^{-13} \text{ sec} ,$$

$$\tau_{D^0} = (6.8^{+2.3}_{-1.8}) \times 10^{-13} \text{ sec} .$$

The results are insensitive to reasonable changes in the values of the cuts (see below) and change by less than 20% when different production models are assumed in the Monte Carlo. (The distribution of l predicted by the Monte Carlo is affected by the production model assumed but little affected by the decay kinematics assumed, whereas the reverse is true for d_{max}; however, l_{eff} and T_{eff} are somewhat affected by both.) The Monte Carlo used agreed well with all features of the data, for example those illustrated in Fig. 15, viz., the total charged momentum in the event and the total visible momentum in the decay. The curves in Figs. 12 and 13 represent the distributions expected with these lifetimes.

Table III gives the lifetime determined from the means of the experimental distributions for each of the four pa-

TABLE III. Lifetimes of charged and neutral charmed particles and their ratios, as determined by various methods explained in the text.

Method	$\tau^{\pm}$ (10^{-13} sec)	τ^0 (10^{-13} sec)	$\dfrac{\tau^{\pm}}{\tau^0}$
(a) Reconstructed decays[a]			
I. $\langle l_{eff} \rangle$	$9.5^{+4.6}_{-2.7}$	$7.2^{+4.4}_{-2.2}$	1.3
(b) All decays			
II. $\langle T_{eff} \rangle$	$6.5^{+2.3}_{-1.7}$	$5.5^{+2.0}_{-1.5}$	1.2
III. $\langle d_{max} \rangle$	$9.8^{+4.0}_{-2.7}$	$6.5^{+2.8}_{-2.1}$	1.5
IV. $\langle l \rangle$	$7.2^{+2.5}_{-1.8}$	$7.1^{+2.4}_{-1.7}$	1.0
V. $\langle l_{eff} \rangle$	$7.2^{+2.5}_{-1.8}$	$6.5^{+2.3}_{-1.6}$	1.1
Maximum-likelihood calculation	$7.2^{+2.3}_{-2.0}$	$6.8^{+2.3}_{-1.8}$	1.1

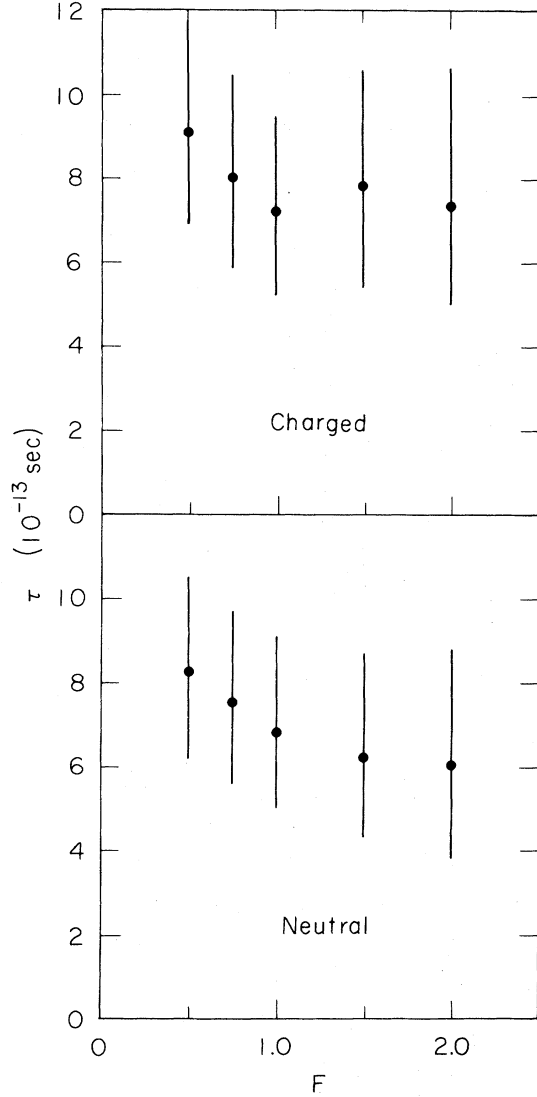[a]Eleven charged and eight neutral decays.

FIG. 16. Effect of changing the cut parameters on the lifetimes determined using the maximum-likelihood method. Cuts are $d_{max} > F \times 100$ μm, $d_2 > F \times 40$ μm, and $l > F \times 500$ μm.

likelihood method remains consistent with the original result.

For constrained decays, in which all the decay products are detected, the momentum, P, of the charmed particle is known. For these events the mean lifetime is given by

$$\tau = \frac{1}{N} \sum_{i=1}^{N} \left[\frac{l_{eff}M}{Pc} \right]_i .$$

Figure 17 shows the mass distribution for all Cabibbo-favored $D^{\pm}$ decay modes (including K^0's and/or one measured π^0) where the decaying particle is required to point back to the primary vertex in the optic plane (azimuthal angle) to within 60 mrad. Only combinations consistent with the track ionization observed in the bubble chamber and the Čerenkov signals detected downstream have been included. All of these decays are consistent with charged D decays and 11 are selected as identified and fully reconstructed, based on a χ^2 test involving the calculated in-
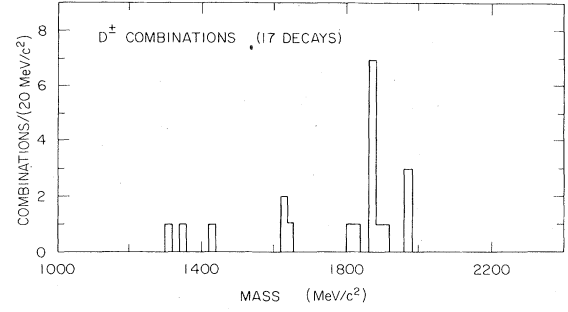

FIG. 17. Invariant mass for Cabibbo-favored $D^{\pm}$ decays. All decays pointing to the primary vertex including those containing one reconstructed π^0 or a visible K_S^0 are included. Particle-identification information has been used. The error on the mass is required to be less than 30 MeV/c^2 for a combination to be included. The decays producing the three combinations above 1950 MeV/c^2 are all consistent with the D mass when particle-mass assignments are changed.

variant mass and azimuthal angle of the meson (the error on the mass was required to be less than 30 MeV/c^2). Eight neutral decays were similarly identified from the neutral decay sample. Table IV lists the properties of these fully reconstructed decays. Ten of the 19 fully reconstructed decays have identified kaons; eight are $K^{\pm}$ and two are K_S^0.

In order to obtain the lifetime of the $D^{\pm}$, the charged-charmed-particle lifetime value of $(7.2^{+2.3}_{-2.0}) \times 10^{-13}$ sec

TABLE IV. Properties of the 8 fully reconstructed D^0 decays and 11 fully reconstructed $D^{\pm}$ decays. The underlined symbols denote the identified particles ($C = $ Čerenkov, $i = $ ionization, $d = $ delta ray).

Roll-frame	Decay mode	Mass (MeV/c^2)	P (GeV/c)	τ (10^{-13} sec)
	(a) D^0			
437-27	$\underline{K}\,\bar{c}\pi^+$	1849±23	8.8	14.0
944-15	$K^+\pi^+\pi^-\pi^-\pi^0$	1880±22	9.7	5.6
994-845	$K^+\pi^+\underline{\pi}\,\underline{c}\,\underline{\pi}\,\overline{i}\,\pi^0$	1833±12	9.9	5.9
1285-919	$\underline{K}\,\underline{c}\pi^+\underline{\pi}\,\overline{i}\,\pi^-$	1873±18	11.4	22.2
1997-398	$\underline{K}\,\bar{c}\pi^-\pi^+\pi^+$	1841±18	7.8	3.5
2529-268	$\underline{K}\,\underline{c}\pi^+\pi^-\pi^-$	1808±17	11.4	1.9
2567-64	$\underline{K}\,^0\underline{\pi}\,_i^+\underline{\pi}\,\overline{c}$	1882±16	6.0	2.1
2652-714	$K^-\underline{\pi}\,\overline{d}\,\pi^+\pi^+$	1884±10	9.1	2.3
Average		1859±5		$7.2^{+4.4}_{-2.2}$
	(b) $D^{\pm}$			
596-237	$K^-\pi^+\pi^+\pi^0$	1832±15	9.6	9.4
781-275	$K^+\underline{\pi}\,\overline{i}\,\underline{\pi}\,\overline{c}$	1871±9	8.1	7.1
916-16	$\underline{K}\,\underline{c}\pi^-\pi^-$	1887±9	8.7	2.4
958-596	$K^+\pi^-\pi^-$	1869±9	7.2	4.9
1293-147	$K^-\pi^+\pi^+\pi^0$	1802±22	6.0	30.0
1303-179	$\underline{K}\,\underline{c}\pi^-\pi^-$	1864±9	10.9	3.2
1415-225	$\underline{K}\,\bar{c}\pi^+\underline{\pi}\,_i^+$	1862±13	7.4	10.3
1795-159	$K^+\underline{\pi}\,\overline{c}\pi^-$	1917±21	16.9	0.1
1893-388	$\underline{K}\,\underline{c}\pi^-\pi^-$	1878±20	6.1	5.8
1914-741	$\underline{K}\,^0\pi^+\pi^-\pi^-$	1876±26	11.1	19.9
2332-897	$K^+\pi^-\underline{\pi}\,\overline{i}$	1871±26	6.6	11.0
Average		1869±4		$9.5^{+4.6}_{-2.7}$

has to be slightly modified to take into account any contamination due to $\Lambda_c^+ \overline{D}$ or $\Lambda \overline{D} F$ production, estimated to be $(35\pm20)\%$ in our experiment (see Sec. IV C). The lifetime of the $D^\pm$ is changed very little from that measured for the charged decays and the value becomes

$$\tau_{D^\pm} = (7.4^{+2.3}_{-2.0}) \times 10^{-13} \text{ sec} .$$

Here we assumed $\tau_{\Lambda_c^+}$ to be 2×10^{-13} sec and the Λ_c^+ and F to have the same branching ratio to one prong as the charged D. If 10% of the charm cross section was $F^+ F^- X$, then the effect of this would be to raise the $\tau_{D^\pm}$ by $< 0.2 \times 10^{-13}$ sec for an F lifetime less than the $\tau_{D^\pm}$.

Using the value of $\tau_{D^0} = (6.8^{+2.3}_{-1.8}) \times 10^{-13}$ sec, we obtain

$$\frac{\tau_{D^\pm}}{\tau_{D^0}} = 1.1^{+0.6}_{-0.3} .$$

B. Charm-production cross section

The sensitivity of the experiment, measured in events/nb, was determined from the total photon flux and scanning and triggering efficiencies. The incident photon flux was determined by summing the signals from a lead-lucite shower counter positioned in the beam downstream of the bubble chamber. The signals from this counter were accumulated for all beam pulses for which the cameras were ready to trigger. This counter was calibrated using $e^+ e^-$ pairs observed in the bubble chamber and in the pair spectrometer upstream of the bubble chamber. From the charm-event scanning efficiency of $(92\pm4)\%$ and the charm-triggering efficiency of $(87\pm4)\%$ (see Sec. III C) we calculate the sensitivity S to be 2.80 ± 0.28 events/nb. This number was also calculated by comparing the total number of hadronic interactions found in the same sample of film to the total hadronic cross section, corrected for scanning and triggering efficiencies, yielding a sensitivity of 2.74 events/nb.

A production- and decay-model-independent lower limit to the number of charm events produced, N_c^{evt}, is the total observed number of events with definite evidence for charm, ignoring the efficiency corrections, etc. From the 62 charm events found (see Sec. III B) and S, we find (with 90% confidence) that the charm-production cross section σ_{charm} is greater than 17 nb.
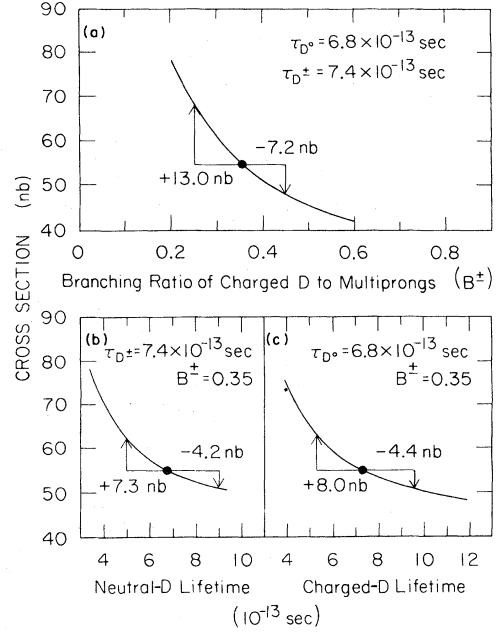

FIG. 18. Dependence of the total-charm cross section on (a) branching ratio of $D^\pm$ to multiprongs, (b) neutral-D lifetime, and (c) charged-D lifetime.

This absolute lower limit can be refined by taking into account the inefficiencies of detection. We choose to assign a detection efficiency to each decay in order to explicitly separate production and decay systematics. The details of this procedure are given in the Appendix. We find a lower limit to the number of charm events in our experiment by assuming all charm is produced via $D\overline{D}$ pair production so that the number of events is one-half the number of decays. This yields $N_c^{\text{evt}} = 117\pm16$ (statistical error only). We do observe evidence for associated $\overline{D}\Lambda_c^+$ production, however, so this is truly a lower limit. We can obtain a direct measurement by counting $\overline{D}$'s, since in either case ($\overline{D}\Lambda_c^+$ or $D\overline{D}$) we will have one. However, since many of our neutral D's are $D/\overline{D}$ ambiguous, we obtain an upper limit of 175 ± 28 events if we assume all these ambiguous decays may be $\overline{D}$. We are ignoring F production as there is no evidence for any in this experiment (see Sec. IV C). The best value between the upper and lower limits can be obtained if we can estimate the

TABLE V. Various sources contributing to the total-charm—cross-section error.

	Contribution to $\Delta\sigma_c$ upwards (nb)	Contribution to $\Delta\sigma_c$ downwards (nb)
Statistical errors	10.5	10.5
Uncertainty between upper and lower limits to N_c^{evt}	6.6	14.0
Uncertainty in branching ratio of charged decays to multiprongs	13.0	7.2
Uncertainty in τ_{D^0}	7.3	4.2
Uncertainty in $\tau_{D^\pm}$	8.0	4.4
Uncertainty in S	6.2	5.3

fraction of $D^0/\bar{D}^0$ ambiguous decays which are $\bar{D}^0$. We do this in the Appendix and find $N_c^{\text{evt}} = 157 \pm 29$, and thus $\sigma_{\text{charm}} = 56$ nb.

This value is sensitive to several parameters, the most important of which are the multiprong branching ratio for charged decays, τ_{D^0} and $\tau_{D^\pm}$. The variation in cross section due to changes in these parameters is demonstrated in Fig. 18. In calculating the quoted cross-section value, we used the lifetimes measured in this experiment (see Sec. IV A). The values of the charm multiprong branching ratios used were $B^0(\text{multiprongs}) = 0.87 \pm 0.05$ and $B^\pm(\text{multiprongs}) = 0.35 \pm 0.10$ (how these values were obtained is described in the Appendix). Taking into account all the various sources contributing to the cross-section error (see Table V), we obtain the total cross section to be[10]

$$\sigma_{\text{charm}} = 56^{+24}_{-23} \text{ nb} .$$

C. Production mechanisms

Various mechanisms for photoproduction of charmed particles have been proposed.[11] Tests of these models can be made using the total charm cross section, its dependence on beam energy, and distributions of various kinematic parameters of the charmed particles. Also, the data can be used, as presented below, to determine the contributions of associated production of charmed mesons accompanied by charmed baryons and of pair production of charmed mesons.

1. Signals for charmed particles in invariant-mass distributions

About one third of the observed decays have invariant masses and transverse momentum balance consistent with Cabibbo-allowed decays of D mesons in which all the products are detected and measured. Eight of these have $K^\pm$ identified by the Čerenkov counters. The distribution of invariant mass in Fig. 17, using all of the charged decays with transverse momentum balance, shows a clear peak at the D mass with a background estimated to be only about one event.

The corresponding plot in the region of the F meson is shown in Fig. 19. It can be seen that the observed peak at 2040 MeV/c^2 is mainly due to the contribution of D mesons when one of the decay pions is assigned a kaon mass; when the fully reconstructed D mesons are removed from the sample no peak remains.

Among the seen decays there is no fully reconstructed Λ_c^+, but for five of the seven positive decays, Λ_c^+ (unconstrained) is not ruled out. A search for charmed-particle masses at the second decay vertices, or, where they were undetected, among the particles at the production vertex, yielded no significant signal. The number of combinations which must be tried is generally large and gives a substantial background. However, some characteristics of the events can sometimes be used to identify the second charmed particles indirectly.

That the majority of the observed decays are D mesons is consistent with the numbers of each decay mode observed. Table VI compares our branching ratios, based on
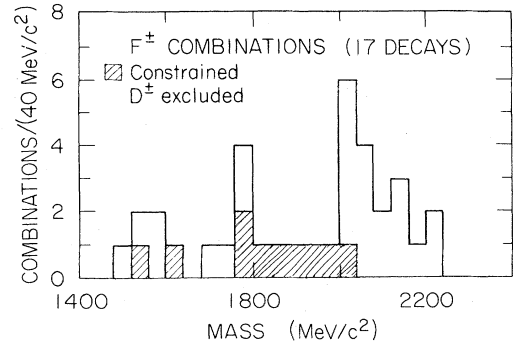

FIG. 19. Invariant mass for charged decays interpreted as Cabibbo-favored $F^\pm$. Only decays which point to the primary vertex are included. Particle-identification information has been used. The hatched histogram shows those combinations remaining after decays interpreted as fully reconstructed D decays have been removed. The enhancement at 2040 MeV/c^2, therefore, is a reflection of D decays which comes when a pion is assigned the kaon mass.

the measured charm cross section and the detection efficiency for each channel, with those already measured.[12] It can be seen that the agreement is good except that we may observe an excess of $D^\pm \rightarrow K^\mp \pi\pi$ decays.

In the $K(n\pi)$ decays (with $n \geq 2$) a signal of four $K^*(890)$ with a background of about 1 is observed, again consistent with known branching ratios for $D^\pm$ decay.

We have looked for a signal near the ϕ mass which would be expected if our $D^\pm$ candidates included a substantial fraction of $F^\pm \rightarrow \phi X^\pm$. We find no signal in a plot of $M_{K^+K^-}$ for all two-body combinations consistent with particle identification.

A search has also been made for $D^{*\pm} \rightarrow D^0 \pi^\pm$ using two methods. First, the 8 fully reconstructed D^0 decays were considered (see Table IV). The effective mass of the $D^0 \pi^\pm$ system was calculated using each charged track (assumed to be a pion) from the primary vertex in turn. No $D^{*\pm}$ mass was found. The second method used all of the 22 unambiguous D^0 decays and the 8 charged/neutral ambiguous decays (assumed to be neutral). For each of these 30 D^0 decays the mass difference between the $D^0 \pi^\pm$ system and the D^0 was estimated by calculating $M_1 - M_2$, where M_1 is the effective mass of the charged tracks from the decay combined with the $\pi^\pm$ and M_2 is the effective mass of just the charged tracks from the decay (all tracks were assumed to be pions). The minimum value for each decay was histogrammed (see Fig. 20). A typical error on this mass difference is 5 MeV/c^2. Note that for real D^* decays this mass difference is ~ 145 MeV/c^2 even when the D^0 decay is not fully reconstructed. The solid curve in Fig. 20 is a Monte Carlo prediction of this minimum mass difference (normalized to 30 decays) for a model with no D^* production (i.e., $\gamma p \rightarrow D\bar{D}N\pi$). Also shown (dashed curve) is the Monte Carlo prediction for $\gamma p \rightarrow D^* \bar{D}^* N\pi$. Eighty-five percent of all real $D^{*\pm} \rightarrow D^0 \pi^\pm$ decays have a mass difference less than 200 MeV/c^2. In this region we see 7 decays compared to an expected number of 2.8 from the $D\bar{D}$ Monte Carlo. This corresponds to a signal of 4.2 ± 2.6 decays. Correcting for the 15% of the signal which is above 200 MeV/c^2, there

TABLE VI. Branching ratios into various final states.

Channel	Number of decays observed	Detection efficiency	Branching ratio[a] (%)	Particle Data Group value (%)
$D^+ \to K^- \pi^+ \pi^+$ $D^- \to K^+ \pi^- \pi^-$	1 } 8 7 }	0.49	11±4	4.6±1.1
$D^+ \to \bar{K}^0 \pi^+ \pi^+ \pi^-$ $D^- \to K^0 \pi^- \pi^- \pi^+$	0 } 1 1 }	0.13	5±5	8.4±3.5
$D^0 \to K^- \pi^+$ $\bar{D}^0 \to K^+ \pi^-$	1 } 1 0 }	0.38	3±3	2.4±0.4
$D^0 \to K^- \pi^- \pi^+ \pi^+$ $\bar{D}^0 \to K^+ \pi^+ \pi^- \pi^-$	2 } 4 2 }	0.51	8±4	4.5±1.3
$D^0 \to \bar{K}^0 \pi^+ \pi^-$ $\bar{D}^0 \to K^0 \pi^+ \pi^-$	1 1	0.06	18±18	4.2±0.8

[a]The calculations of the branching ratio used the branching ratios of D^0 and $D^\pm$ into multiprongs (Ref. 20), B^0 (multiprongs) $=0.87\pm0.05$; $B^\pm$ (multiprongs) $=0.35\pm0.10$.

are therefore 4.9 ± 3.1 $D^{*\pm} \to D^0\pi^\pm$ decays amongst the 30 possible D^0 decays. Furthermore, correcting for the branching ratio of $D^{*\pm} \to D^0\pi^\pm$ and the efficiency for detecting D^0 decays gives 27 ± 18 $D^{*\pm}$ particles produced in the experiment, i.e., the number of $D^{*\pm}$ per charm event is 0.17 ± 0.11. This number is consistent with small D^* production (or none at all). This conclusion is supported by the fact that we see approximately equal numbers of charged and neutral D decays (an excess of neutral decays is expected if there is a significant amount of D^* production).

2. Λ production

If the rate of Λ production were the same in charm as in noncharm events,[13] 1.4 Λ decays would be visible in the charm sample whereas six are observed. The excess could well be from the decay of Λ_c^+ which may decay[14] significantly into Λ or from final states such as $\Lambda \bar{D} F$. However, there is only one visible charm decay in each of the six events and five of these are negative (the other is neutral). The fact that no second vertex is seen in these events is quite consistent with a Λ_c^+ lifetime[15] of $\sim 2 \times 10^{-13}$ sec. Furthermore, these negatives have higher average visible momentum (10.5 GeV/c) than the total positive decay sample (5.34 GeV/c). This is consistent with $\Lambda_c^+ \bar{D}$ production. If we assume that production of $\Lambda \bar{D} F^+$ can be

ignored relative to that of $\Lambda_c^+ \bar{D}$, an estimate of the rate of $\Lambda_c^+ \bar{D}$ production can be made as follows. Assuming that the branching ratio for Λ_c^+ decay to Λ is 50% and using the branching ratio for $\Lambda \to p\pi^-$ (64%) together with a $\Lambda \to p\pi^-$ detection probability of 81% as calculated by a Monte Carlo method, the excess of 4.6 events implies that (40 ± 20)% of the charm events are associated production of $\Lambda_c^+ \bar{D}$.

3. $D/\bar{D}$ ratio

Using the signs of identified kaons and assuming the decays to be D mesons with no Cabibbo-suppressed modes, 18 of the 28 decays were assigned as D^- or $\bar{D}^0$ and 10 as D^+ or D^0. If the excess is interpreted as being due to $\Lambda_c^+ \bar{D}$ production, then (44 ± 22)% of charm production comes from this source. Interpreting the $D/\bar{D}$ ratio as indicative of some associated production is further supported by the differences in the D^+ and D^- momentum distributions. Figure 21 shows the $P_{\min}$ distributions
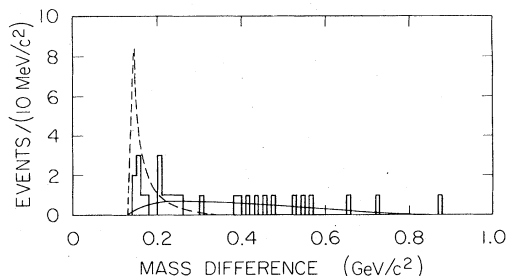
FIG. 20. Minimum mass difference between $D^0\pi^\pm$ system and D^0 (all tracks assumed to be pions). The two curves are Monte Carlo predictions from $\gamma p \to D\bar{D}N\pi$ (solid) and $\gamma p \to D^*\bar{D}^*N\pi$ (dashed).
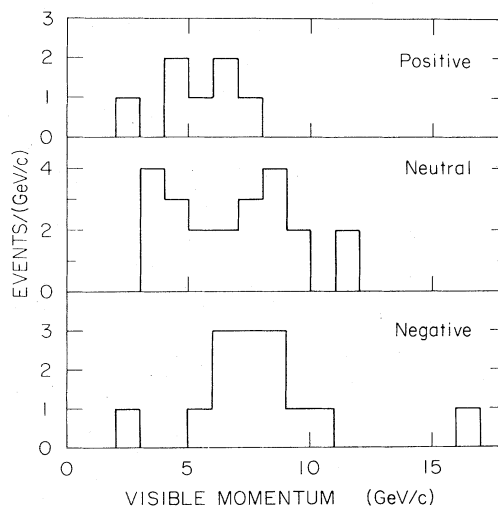
FIG. 21. Visible momentum from positive-, neutral-, and negative-charmed-particle decays.

for each charge; the averages are 8.03 GeV/c for negatives, but only 5.34 GeV/c for positives.

4. Pair production of D^0 and $\bar{D}^0$

Four events are observed in which one neutral decay passes all the selection criteria, and a second decay not necessarily passing the cuts is also neutral. None of these events has a seen Λ decay and three of the four have identified protons at the primary vertex. The assumption that these events are $D^0\bar{D}^0$ pairs sets a lower limit on $D\bar{D}$ production. Correcting for $D^0\bar{D}^0$ detection efficiency, and using a simple statistical model to relate the number of $D^0\bar{D}^0$ pairs to the total number of $D\bar{D}$ pairs, we estimate that $(80^{+20}_{-40})\%$ of the events contain $D\bar{D}$ pairs.

5. Events with two charm decays

The two events found in which both decays passed the cuts are consistent with the estimate (summarized in Sec. IV C 7), that $(65\pm20)\%$ of the charm events contain $D\bar{D}$ pairs.

6. The rate of K^0 production

If K^0's were produced at the same rate in the charm events as in the others[13] there should be two K^0's seen in the charm sample whereas six are observed (two in one event). After corrections for unseen decay modes and escape from the chamber this corresponds to 21 K^0's produced. This is again consistent with expectations from pure $D\bar{D}$ production but can also be explained by other mechanisms.

7. Conclusion on the fraction of $D\bar{D}$ production

Putting together all the indirect evidence presented above for non-$D\bar{D}$ contributions to our charm sample, we conclude that $(65\pm20)\%$ of the charm events contain $D\bar{D}$ pairs.[16] The remaining $(35\pm20)\%$ could be due to either $\Lambda_c^+\bar{D}$ or $\Lambda F^+\bar{D}$ production; however, phase-space arguments would favor the former.

8. Longitudinal and transverse momentum

The distributions of longitudinal momentum and transverse momentum for the fully reconstructed decays are shown in Fig. 22. The D's carry on average 9.09 GeV/c ($\sim0.45E_\gamma$). These distributions are consistent with models used above for the lifetime and cross-section determinations.

9. Comparison of the data with model predictions

This experiment gives a measurement of the total charm cross section near threshold which is shown in Fig. 23, together with data from other experiments at higher energies.[17] Also shown are various theoretical predictions for the dependence of the cross section on beam energy. Of these, the results favor the photon-gluon-fusion models.

Given that their photon-gluon-fusion model may be appropriate for calculating the cross section, Babcock,
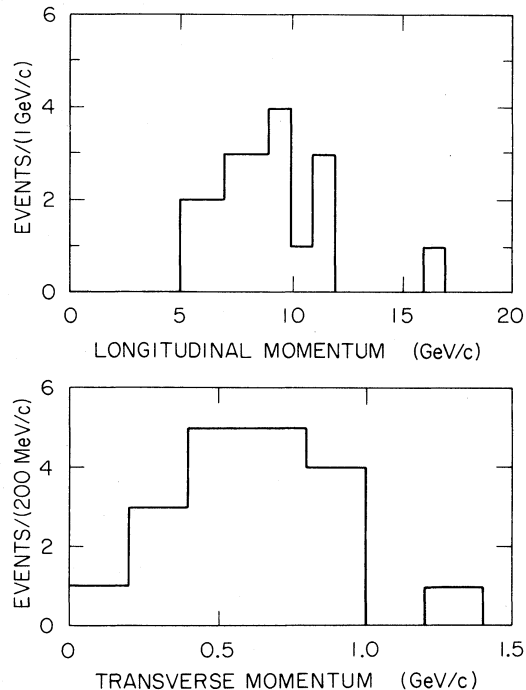

FIG. 22. Longitudinal- and transverse-momentum distribution of constrained decays.

Sivers, and Wolfram show that a measurement at 20 GeV should give good discrimination between several assumed gluon distributions. Our cross section favors a harder gluon distribution than given by the "naive" form, $xG(x)=3(1-x)^5$, where x is the fraction of the proton momentum carried by the gluon.
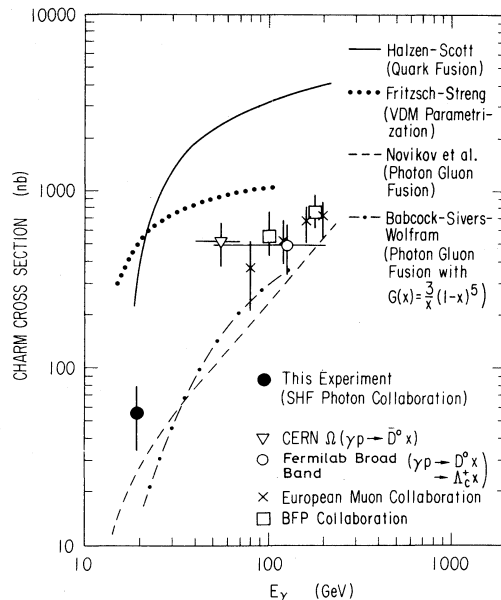

FIG. 23. Charm-production cross section as a function of energy. The curves are predictions from the models indicated.[11] Other data points are from Ref. 17.

In principle a further test of photon-gluon-fusion models is available using kinematic distributions of the observed charmed particles. However, because the available phase space is limited at our energy, predictions are relatively insensitive to the exact form of the gluon distribution. In fact, the largest variations in the model predictions arise from uncertainties in the way in which the charmed quarks produced near threshold fragment into charmed particles.

V. DISCUSSION AND CONCLUSIONS

From an experiment involving $\sim 580 \times 10^3$ hadronic events produced in hydrogen by 20-GeV γ rays, 51 clear decays of charmed particles have been selected from 72 decays. The background from all sources is less than one charged and one neutral in our sample of charm decays.

New results on the lifetimes of the charged and neutral D mesons have been obtained,

$$\tau_{D^\pm} = (7.4^{+2.3}_{-2.0}) \times 10^{-13} \text{ sec},$$

$$\tau_{D^0} = (6.8^{+2.3}_{-1.8}) \times 10^{-13} \text{ sec},$$

which are in good agreement with our results published earlier,[1] based on about half our present statistics. The charged-D lifetime is in good agreement with that obtained by other experiments,[18] while the D^0 lifetime is somewhat longer by about 1.5σ from the "best estimate" value obtained recently.[15] Two types of mechanisms are supposed to contribute to the decay of D mesons.[19] These are due to (a) spectator diagrams in which the charged quark decays without affecting the other quark in the meson, and (b) nonspectator diagrams in which both quarks participate in the decay via the exchange of a W boson. The spectator mechanism affects D^0 and D^+ decays equally, whereas the nonspectator mechanism only applies to D^0 decays. The deviation of $\tau_{D^\pm}/\tau_{D^0}$ from unity is therefore a measure of the relative amounts of nonspectator and spectator contributions to the decay of the D^0. Our value of $\tau_{D^\pm}/\tau_{D^0} = 1.1^{+0.6}_{-0.3}$ is in line with the spectator mechanism dominating.

No uniquely identified Λ_c^+ or $F^\pm$ decays were found, however, indirect evidence is consistent with some Λ_c^+ production and we obtain

$$\frac{\sigma(\gamma p \rightarrow \Lambda_c^+ X)}{\sigma(\gamma P \rightarrow D\bar{D}X) + \sigma(\gamma p \rightarrow \Lambda_c^+ X)} = (35 \pm 20)\% .$$

In the case of F production, we have no direct or indirect evidence that suggests that F's are produced in our experiment. Indeed, we have good evidence that the great majority of the charged decays we see are in fact $D^\pm$. We cannot put good upper limits to $F^\pm$ production because too few will survive our cuts if the F has a short lifetime ($< 3 \times 10^{-13}$ sec) as suggested by other experiments.[18]

We find only a small amount of $D^{*\pm}$ production (or none at all) suggesting that most of our $D^\pm$ and D^0 particles are produced directly.

Finally, we measure the total photoproduction of charm cross section to be $\sigma_{\text{charm}} = (56^{+24}_{-23})$ nb. The errors are largely due to uncertainties in the lifetimes of the charmed particles, the ratio of the one-prong to multiprong decays of the $D^\pm$, and the large error on the extent of possible Λ_c^+ production. This result is consistent with predictions of various versions of the photon-gluon-fusion model.

APPENDIX

The number of charm events produced, N_c^{evt}, was calculated as follows: Let N_i be the number of produced charmed particles of ith type (such as D^0, Λ_c^+, etc.) and $\phi^i(p)$ be their momentum distribution. Then define $B^i(T)$ to be the branching ratio of type i into decay T (such as constrained two-prong or three-prong decays or uncon-
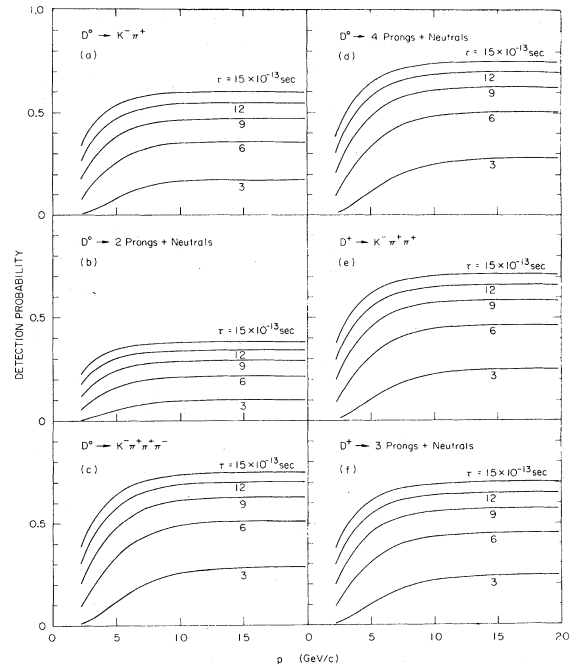

FIG. 24. Detection efficiencies for D mesons into various decay modes as a function of momentum and lifetime. The smallest kinematically allowed D momentum is 2.22 GeV/c for $\gamma p \rightarrow D\bar{D}N$.

strained two-prong decays, etc.) and define $\epsilon^{i}(T,p,\tau^{i})$ to be the detection efficiency of decay T, given that it originated from charmed particle of type i with momentum p and lifetime τ^{i}. This was calculated using a Monte Carlo program. After cuts (i)—(vi) (Sec. III B) were applied to the generated decays, the efficiency ϵ was calculated as the ratio of decays surviving the cuts to the total number generated. Figure 24 shows ϵ as a function of p and τ for various decays of D mesons.

Then the observed momentum distribution of decays of type T, passing the cuts, is given by

$$n_{T}(p) = \sum_{i}^{\text{all sources}} N_{i}B^{i}(T)\phi^{i}(p)\epsilon^{i}(T,p,\tau^{i}) . \tag{A1}$$

Selecting one particular charm particle, say $i = k$, and defining weight w as

$$w(T,p,\tau^{k}) \equiv \frac{1}{\epsilon^{k}(T,p,\tau^{k})} , \tag{A2}$$

we obtain

$$\int dp \, w(T,p,\tau^{k})n_{T}(p) = B^{k}(T) \left[N_{k} + \sum_{i \neq k} N_{i} \frac{B^{i}(T)}{B^{k}(T)} \int dp \, \phi^{i}(p) \frac{\epsilon^{i}(T,p,\tau^{i})}{\epsilon^{k}(T,p,\tau^{k})} \right] . \tag{A3}$$

Equation (A3) becomes particularly simple if only a single source k contributes. In this case Eq. (A3) implies that summing the weights of all observed decays of type T in the experiment, we obtain an estimate of $N_{k}B^{k}(T)$.

If we assume that only D mesons and Λ_{c}^{+} baryons are produced, then all negative decays can originate only from D^{-} mesons and the positive decays can originate either from D^{+} or Λ_{c}^{+}. The neutral decays divide into three categories, depending on whether they were identified as D^{0}, $\overline{D}^{0}$ or were ambiguous between D^{0} and $\overline{D}^{0}$ (see footnote a, Table VII). In Table VII we divide all the decays passing the cuts into these five categories. The sums of the weights are shown; they were calculated from the Monte Carlo assuming that all the decays were D mesons. The last column of Table VII gives the physical meaning of the weight sums as implied by Eq. (A3). These have a simple meaning for categories 1, 2, and 4 because only one charmed particle contributes. The category of $D^{0}/\overline{D}^{0}$ ambiguous decays (category 3) corresponds to a sum of two terms (D^{0} and $\overline{D}^{0}$). However, since for a given momentum the detection efficiency of a neutral decay does not depend on whether the decaying particle is a D^{0} or $\overline{D}^{0}$, this sum, as shown in Table VII, has a simple form. The positive decays (category 5) are more complicated. Their weight sum also corresponds to a sum of two terms (D^{+} and Λ_{c}^{+}). This time, however, the term corresponding to Λ_{c}^{+} is equal to the number of Λ_{c}^{+}'s produced ($N_{\Lambda_{c}^{+}}$) multiplied by the branching ratio of Λ_{c}^{+} into multiprongs and also multiplied by the ratio of Λ_{c}^{+} and D^{+} detection efficiency averaged over the Λ_{c}^{+} momentum spectrum (see footnote c, Table VII). We will discuss this term later. As can be seen from Table VII the sum of weights of all neutral decays divided by the branching ratio of D^{0} into multiprongs and added to the sum of weights of all charged decays divided by the branching ratio of $D^{\pm}$ into multiprongs,

TABLE VII. Decay categories and their weighted numbers.

Cat. no.	Decay category	Source	Number[d] of decays passing cuts	Weighted number W_{CAT}	Right-hand side of Eq. (A3)
1	two-, four-, · · · prong decays identified as D^{0a}	D^{0}	3	6.4 ± 3.7	$N_{0}B^{0}(\text{multiprongs})\alpha^{b}$
2	two-, four-, · · · prong decays identified as $\overline{D}^{0a}$	$\overline{D}^{0}$	6	16.2 ± 7.2	$N_{\overline{0}}B^{0}(\text{multiprongs})\overline{\alpha}^{b}$
3	two-, four-, · · · prong decays ambiguous	$D^{0},\overline{D}^{0}$	17	57.4 ± 13.9	$B^{0}(\text{multiprongs})[N_{0}(1-\alpha)+ N_{\overline{0}}(1-\overline{\alpha})]$
4	negative decays	D^{-}	16	31.8 ± 7.6	$N_{-}B^{\pm}(\text{multiprongs})$
5	positive decays	D^{+},Λ_{c}^{+}	9	18.3 ± 5.8	$(N_{+}+N_{\Lambda_{c}^{+}}g)B^{\pm}(\text{multiprongs})^{c}$

[a]The neutral decay is identified as D^{0} or $\overline{D}^{0}$ either (i) by being constrained to a Cabibbo-allowed D^{0} decay mode, or (ii) by one of the tracks being identified as a K^{+} or K^{-} by the Cerenkov counter, or (iii) by the fact that there is another charged charm decay in the event.

[b]α, ($\overline{\alpha}$), is the probability that a neutral decay is identified as a D^{0} ($\overline{D}^{0}$) as described in footnote a.

[c]g is defined as

$$g \equiv \frac{B^{\Lambda_{c}^{+}}(\text{multiprongs})}{B^{\pm}(\text{multiprongs})} \int dp \phi^{\Lambda_{c}^{+}}(p) \frac{\epsilon^{\Lambda_{c}^{+}}(\text{multiprongs},p,\tau_{\Lambda_{c}^{+}})}{\epsilon^{\pm}(\text{multiprongs},p,\tau^{\pm})} .$$

[d]The charged/neutral ambiguous decays are added to categories 3, 4, and 5 as fractional events according to their ambiguous topologies.

$$A \equiv \frac{(W_1 + W_2 + W_3)}{B^0(\text{multiprongs})} + \frac{(W_4 + W_5)}{B^{\pm}(\text{multiprongs})},$$

is equal to the total number of charmed particles produced ($N_c = N_0 + N_{\bar{0}} + N_+ + N_- + N_{\Lambda_c^+}$) corrected by an extra term which arises due to the fact that the weights were calculated assuming that all the decays were D mesons,

$$A = N_c - N_{\Lambda_c^+}(1 - g) \qquad (A4)$$

(see footnote c, Table VII for a definition of g).

Since there are two charmed particles produced per event, the number of charm events, N_c^{evt}, is given by

$$N_c^{\text{evt}} = \frac{N_c}{2} = \frac{A}{2} + \frac{1}{2}N_{\Lambda_c^+}(1 - g). \qquad (A5)$$

If there were no Λ_c^+'s produced, the number of events containing charm would be $A/2$. However, there is evidence for Λ_c^+ production (see Sec. IV C) and the second term in Eq. (A5) cannot be neglected. This term depends on the number of Λ_c^+'s produced and also on their decay properties as expressed in the factor g. The relative detection efficiency of Λ_c^+ compared to D^+ averaged over a reasonable Λ_c^+ momentum spectrum is less than 0.3 for $\tau_{\Lambda_c^+} < 3 \times 10^{-13}$ sec. This means that g is most likely less than 1 and in such case $A/2$ provides a lower limit to the number of charm events N_c^{evt}. This lower limit is 117 ± 16 (errors are statistical).

An upper limit to N_c^{evt} was obtained as follows. Note that

$$N_c^{\text{evt}} = N_{\bar{0}} + N_- = N_0 + N_+ + N_{\Lambda_c^+}.$$

But from Table VII we see that

$$B \equiv \frac{W_2 + W_3}{B^0(\text{multiprongs})} + \frac{W_4}{B^{\pm}(\text{multiprongs})}$$

$$= N_{\bar{0}} + N_- + N_0(1 - \alpha) \qquad (A6)$$

(see footnote b, Table VII for a definition of α). Therefore,

$$N_c^{\text{evt}} = B - N_0(1 - \alpha) \qquad (A7)$$

and B provides an upper limit of 175 ± 28 events.

Equation (A7) yields the actual number of produced events, N_c^{evt}, when α is known. We can estimate α by assuming that the fractions of D^0 and $\bar{D}^0$ contained within category 3 are the same as those within categories 1 and 2 (i.e., $\alpha = \bar{\alpha}$). Then we obtain $\alpha = 0.28$ and $N_0 = 26.3$. Using these values in Eq. (A7) yields our best estimate of the value of N_c^{evt},

$$N_c^{\text{evt}} = 157 \pm 29.$$

In calculating the quoted number of events, we used the lifetimes measured in this experiment. The branching fractions of D^0 and $D^{\pm}$ were taken from Ref. 20. However, care has been taken since the results quoted in Ref. 20 for branching ratios include $K_S^0 \to \pi^+ \pi^-$. To unfold this effect we assumed that 85% of the decays are Cabibbo favored and included uncertainty of this assumption in the errors. The values obtained were $B^0(\text{multiprongs}) = 0.87 \pm 0.05$ and $B^{\pm}(\text{multiprongs}) = 0.35 \pm 0.10$.

---

*On leave from Technion—Israel Institute of Technology, Haifa, Israel.

†Present address: College de France, Paris, France.

‡Present address: Southeastern Massachusetts University, N. Dartmouth, Massachusetts.

[1]K. Abe *et al.*, Phys. Rev. Lett. **48**, 1526 (1982); K. Abe *et al.*, *ibid.* **51**, 156 (1983).

[2]Z. D. Farkas *et al.*, IEEE Trans. Nucl. Sci. **NS-22**, 1299 (1975); **NS-24**, 1827 (1975).

[3]J. C. Kent, Ph.D. thesis, University of California, Berkeley, 1983, Report No. UCPPG83-05-20.

[4]J. D. Ferrie *et al.*, Nucl. Instrum. Methods **203**, 223 (1982).

[5]R. C. Field *et al.*, Nucl. Instrum. Methods **200**, 237 (1982).

[6]A. Bevan *et al.*, Nucl. Instrum. Methods **203**, 159 (1982).

[7]J. E. Brau *et al.*, Nucl. Instrum. Methods **196**, 403 (1982).

[8]J. T. Carroll *et al.*, Report No. SLAC-PUB-2726, 1981 (unpublished); in *Proceedings of the Topical Conference on the Application of Microprocessors to High Energy Physics Experiments, CERN, Geneva, Switzerland, 1981* (CERN Report No. 81-07, 1981); P. Rankin, Ph.D. thesis, Imperial College, London, 1982, Report No. HEP-T-99.

[9]S. E. Derenzo and R. H. Hildebrand, Nucl. Instrum. Methods **69**, 287 (1969).

[10]Kent's thesis (Ref. 3) contains further discussion of this method of cross-section determination. The central value for the cross section reported in this thesis differs from that reported in this paper because of (a) use of a smaller preliminary data sample, (b) use of world average D^0 and D^+ lifetime values rather than those measured in this experiment, (c) neglecting Cabibbo-unfavored decay modes in estimating the $D^{\pm}$ one-prong branching ratio, and (d) including a crude estimate of $F^{\pm}$ in calculating lower and upper limits to N_c^{evt}.

[11]F. Halzen and D. M. Scott, Phys. Lett. **72B**, 404 (1978); H. Fritzsch and K. M. Streng, *ibid.* **72B**, 385 (1978); V. A. Novikov, M. A. Shifman, A. I. Vainshtein, and V. I. Zakharov, Nucl. Phys. **B136**, 125 (1978); J. Babcock, D. Sivers, and S. Wolfram, Phys. Rev. D **18**, 162 (1978).

[12]Particle Data Group, Phys. Lett. **111B**, 1 (1982).

[13]K. Abe *et al.*, Phys. Rev. D **29**, 1877 (1984).

[14]J. G. Korner, G. Kramer, and J. Willrodt, Z. Phys. C **2**, 117 (1979).

[15]G. Kalmus in *Proceedings of the 21st International Conference on High Energy Physics, Paris, 1982,* edited by P. Petiau and M. Porneuf [J. Phys. (Paris) Colloq, **43**, C3-431 (1982)]; C. Jarlskog, in *Proceedings of the International Europhysics Conference on High Energy Physics, Brighton, 1983,* edited by J. Guy and C. Costain (Rutherford Appleton Laboratory, Chilton, Didcot, United Kingdom ,1984); N. W. Reay, in

Proceedings of the 1983 International Symposium on Lepton and Photon Interactions at High Energies, Ithaca, New York, edited by D. G. Cassel and D. L. Kreinick (Cornell University, Ithaca, 1984).

[16]C. A. Woods, Ph.D. thesis, Imperial College, London, 1983, Report No. HEP-T-111.

[17]D. Aston *et al.*, Phys. Lett. **94B**, 113 (1980); P. Avery *et al.*, Phys. Rev. Lett. **44**, 1309 (1980); J. J. Russell, *et al.*, *ibid.* **46**, 799 (1981); J. J. Aubert *et al.*, Nucl. Phys. **B213**, 31 (1983); A. R. Clark *et al.*, Phys. Rev. Lett. **45**, 682 (1980).

[18]N. Ushida *et al.*, Phys. Rev. Lett. **45**, 1053 (1980); N. Ushida *et al.*, *ibid.* **48**, 844 (1982); E. Albini *et al.*, Phys. Lett. **110B**, 339 (1982); M. Aguilar-Benitez *et al.*, *ibid.* **122B**, 312 (1983);

A. Badertscher *et al.*, *ibid* **123B**, 471 (1983); J. A. Jaros, in *Physics at Very High Energies,* proceedings of the Summer Institute on Particle Physics, SLAC, 1982, edited by A. Mosher (SLAC Report No. 2595), p. 595.

[19]N. Cabibbo and L. Maiani, Phys. Lett. **79B**, 109 (1978); N. Cabibbo, G. Corbo, and L. Maiani, Nucl. Phys. **B115**, 93 (1979); B. Guberina *et al.*, Phys. Lett. **89B**, 111 (1979); W. Bernreuther, O. Nachtmann, and B. Stech, Z. Phys. C **4**, 257 (1980); H. Fritzsch and P. Minkowski, Phys. Lett. **90B**, 455 (1980); M. Bander, B. Silverman, and A. Soni, Phys. Rev. Lett. **44**, 7 (1980).

[20]G. Trilling, Phys. Rep. **75**, 57 (1981).

FIG. 10. Photographs of two events taken by the high-resolution camera. Note that the time shown is the actual flight time, not an effective lifetime. (a) Neutral fully reconstructed $\overline{D}^0 \rightarrow K^+\pi^+\pi^-\pi^-$. (b) Charged fully reconstructed $D^- \rightarrow \pi^- K^+\pi^-$.